Supporting Information

Amino Decorated Adenine Based Metal-organic Framework for multi-faceted applications

Alehegn Eskemech,[a] Diksha Gambhir,[a] Harpreet Kaur,[a] Anirban Karmakar,[b] and Rik Rani Koner*[c]

[a.]School of Chemical Sciences, Indian Institute of Technology Mandi, Mandi 175075, Himachal Pradesh, India.

[b.]Centro de Química Estrutural, Instituto Superior Técnico, Universidade de Lisboa, Av. Rovisco Pais, 1049–001 Lisbon, Portugal

[c.]School of Mechanical and Materials Engineering, Indian Institute of Technology Mandi, Mandi 175075, Himachal Pradesh, India

Materials and General Methods

All the chemicals were purchased commercially and used as received. $Zn(NO_3)_2.6H_2O$, adenine and 5-aminoisophthalic acid were purchased from Sigma Aldrich. Antibiotics: tetracycline (TC), doxycycline (Doxy) nitrofurazone (NFZ), nitrofurantoin (NFT), chloramphenicol (CAP), thiamphenicol (THI) and sulfadiazine (SDA) were purchased from TCI Chemicals (India) Pvt. Ltd. Furazolidine (FZD) was purchased from Central Drug House (P) Ltd, CDH. The explosives and other analytes, 2,4,6-trinitrophenol (TNP), 2,4-dinitrophenol (2,4-DNP), 4-nitrophenol (4–NP), 2-nitrophenol (2-NP), 2,4,6-trinitrotoluene (TNT), 2,4-dinitrotoluene (2,4-DNT) nitrobenzene (NB), chlorobenzene (CB), phenol (PHL), methylbenzene (MB), and nitromethane were purchased from Sigma Aldrich.

Powder X-ray diffraction (PXRD) data was collected over the 2θ range of 5–50° using Rigaku Smart Lab, X-ray diffractometer with Cu-Kα radiation (λ = 1.54184 Å) at 45 kV and 100 mA at room temperature with a scanning rate of 2° min^{-1}, a scan step of 0.02. UV-vis spectra were obtained from SHIMADZU UV-2450 spectrophotometer in the range of 200-800 nm at room temperature. Perkin Elmer (UV-2450) was used to record the solid-state UV-vis spectra. Cary Eclipse fluorescence spectrometer (Agilent Technologies) was used to record the fluorescence spectra. Thermogravimetric analysis (TGA) was performed using instrument model no. NETZSCHSTA 449 F1 JUPITER in a range from room temperature to 900 ℃ with a heating rate of 10 ℃ min^{-1} under N_2 atmosphere. The morphology was analysed by FEI NOVA NANO SEM–450 field emission scanning microscopy (FE-SEM). Thermo Fischer NEXSA instrument was used to perform the X-ray photoelectron spectroscopic (XPS) measurements using Al-Kα as an X-ray source with an energy of 1486.68 eV. The Quantachrome Autosorb-iQ-MP-XR system was used to obtain N_2 adsorption-desorption isotherms at 77 K. The CHNS analyser (UNICUBE, Elementar) was used to perform elemental analysis.

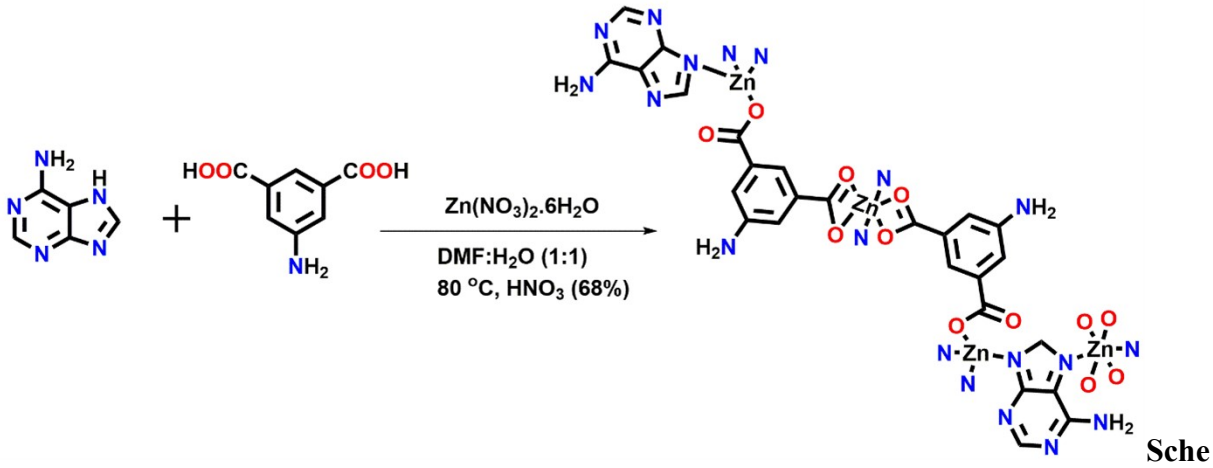

Scheme S1. Synthesis scheme of Zn-MOF

Activation process of Zn-MOF

The as-synthesized Zn-MOF was activated with ethanol. Typically, the as-synthesized Zn-MOF crystals were washed three times with DMF. Thereafter, the Zn-MOF was soaked in 30 ml of ethanol for four hrs and this process was repeated for three times. Subsequently, fresh ethanol was added and allowed to soak for 24 hours. Finally, the ethanol-exchanged Zn-MOF was dried at 80 ^{o}C for 24 h, followed by 100 ^{o}C for 8 h.

Experimental Procedures

Fluorescence Detection Experiments

The excellent luminescence properties and highly stable nature of Zn-MOF in the aqueous medium motivated us to explore its potential for detecting antibiotics and nitroaromatic explosives. The Zn-MOF was finely ground into powdered form to enhance the uniformity and dispersibility in water. Then, the ground Zn-MOF was dispersed in deionized water with a concentration of 0.5 mg/mL and sonicated for 1.5 h to form a stable MOF suspension. Then, 2.5 mL of Zn-MOF suspension was transferred into a 3 mL cuvette and the fluorescence was measured before and after the incremental addition of selected aromatic explosives using a stock solution of 1 mM.

Particularly, 20 µL of 1 mM of each analyte (4,6 - trinitrophenol (TNP), 2,4 - dinitrophenol (2,4-DNP), 4 - nitrophenol (4-NP), 2 - nitrophenol (2-NP), 2,4,6-trinitrotoluene (TNT) and 2,4-dinitrotoluene (2,4-DNT)) was added each time to 2.5 mL of MOF suspension. For comparison, other aromatic and aliphatic compounds such as phenol (PHL), methylbenzene (MB), chlorobenzene (CB), nitrobenzene (NB) and nitromethane (NM) were used. A similar procedure was employed for the detection of antibiotics. The used antibiotics are as follows; tetracycline (TC), doxycycline (Doxy), sulfadiazine (SDA), nitrofurans: nitrofurantoin (NFT), nitrofurazone (NFZ) and furazolidone (FZD) and chloramphenicol (CAP) and thiamphenicol (THI).

The Fluorescence quenching was determined using equation given below:

$$Quenching\ efficiency(\%) = \frac{(I_0 - I)}{I_0} \times 100\% \qquad (1)$$

Where I_0 and I represent the fluorescence intensity of the Zn-MOF before and after the addition of analytes.

Stern-Volmer (SV) equation: $$I_0/I = 1 + K_{SV}[Analyte] \qquad (2)$$

Where I_0 and I represent the fluorescence intensity of the Zn-MOF before and after the addition of analytes and K_{SV} is the Stern-Volmer or quenching constant.[1, 2]

Limit of Detection (LOD) = $$3\sigma/Slope \qquad (3)$$

Where σ is the standard deviation of the blank measurements of fluorescence emission spectra of Zn-MOF and slope is calculated from the of linear plot of intensity of Zn-MOF versus concentration of analyte added.

For the interference study, firstly the fluorescence emission spectrum of 2.5 mL of MOF suspension was recorded and then 100 μL of one of the analytes (SDA or THI) (1 mM) was added to the MOF suspension and the emission spectra were recorded. Subsequently, 100 μL of the second analyte (NFT, NFZ, Doxy, or TC; stock solution of 1 mM) was introduced and the emission spectra were recorded. Such processes were repeated (the addition of analytes turn by turn) until the total volume of each added antibiotics solution reached 300 μL.

All analytes, antibiotics and explosive solutions, with the concentration of 1 mM, were prepared by dissolving the required amount of analyte into deionized water. The fluorescence spectra were recorded at the excitation wavelength of 314 nm, with emissions in the range of 329 nm to 600 nm. All experiments were conducted at room temperature.

Computational Studies

To understand the mechanism, cluster modelling approach has been applied in this work. Using the crystal structure of the Zn-MOF periodic system, a molecular model containing four Zn centers (four coordinated) has been constructed as shown in Scheme S2. All geometry optimizations were performed with DFT using hybrid B3LYP functional in conjunction with Grimme's D3 empirical dispersion correction along with Becke Johnson damping (D3BJ).[3] The initial geometry input for the cluster model was obtained from the crystal structure of the Zn-MOF. During the geometry optimization, all main-group elements (C, N, O, and H) were described with the Pople's double-ξ basis set with one polarization function on the non-hydrogen atoms, 6-31G(d). Whereas, SDD basis set and associated effective core potential (ECP) was used to describe Zn.[4] The geometry optimizations were performed in gas-phase and the optimized structures were subjected to harmonic vibrational frequency calculations and all positive frequencies verify that they are true stationary points. The electronic energies of the stationary points were improved through single-

point energy calculations with a larger basis triple-ξ basis set 6-311++G(d,p) for all main group elements C, N, O and H and SDD basis set and associated ECP for Zn. All computations involving geometry and energy were performed using Gaussian 09 suite of electronic structure programs.[5]

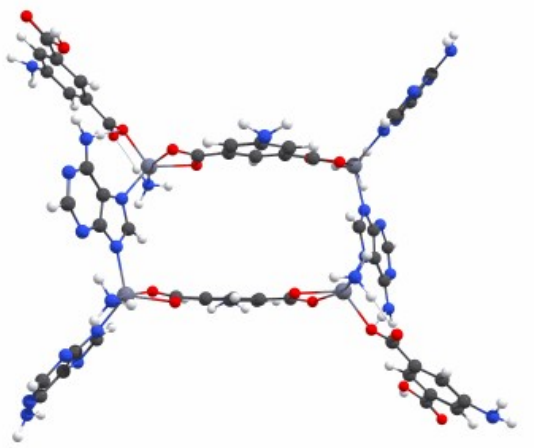

Scheme S2: Zn-MOF molecular model constructed for theoretical calculations

Adsorption Studies

Zn-MOF (8 mg) was immersed into 20 mL of an aqueous solution of any of the antibiotics (NFT, NFZ, TC and Doxy) of a concentration of 10 ppm in a 25 mL of the conical flask. At a specific time interval, 2 mL of aliquot was taken and centrifuged for 20 min at 1200 rpm and the percentage removal of the antibiotics was determined by UV-vis spectrophotometry. NFZ was considered to calculate the maximum adsorption capacity and adsorption kinetics. The adsorption kinetics of antibiotics were fitted to Pseudo-first order and pseudo-second-order models using equation 4&5 respectively.[6, 7]

$$\log\left(q_e - q_t\right) = \log q_e - \frac{k_1 t}{2.303} \qquad (4)$$

$$\frac{t}{q_t} = \frac{1}{k_2 q_e^2} + \frac{t}{q_e} \quad (5)$$

Where q_e is the adsorption capacity at equilibrium (mg/g), q_t is the adsorption capacity at time t (mg/g), k_1 is the rate constant of first order adsorption (min^{-1}) and k_2 is the rate constant of pseudo-second-order adsorption (g/mg min). Different concentrations of NFZ ranging from 10 to 40 ppm were taken and adsorption was performed for next 7 h. The amount of the antibiotics adsorbed on the MOFs at time t and at equilibrium were determined using following equation 6 and 7, respectively.[6]

$$q_e = \frac{(C_o - C_e) \times V}{m} \quad (6)$$

$$q_t = \frac{(C_o - C_t) \times V}{m} \quad (7)$$

where q_e (mg g^{-1}) is the adsorbed amount at equilibrium; C_o and C_e(mg L^{-1}) are the initial and equilibrium concentrations of solution; V (L) is the volume of solution; m (g) is the mass of adsorbent. The adsorption isotherms were examined and data was fitted using Langmuir and Freundlich models using equations 8 and 9.[6, 7]

$$\frac{C_e}{q_e} = \frac{1}{q_m k} + \frac{C_e}{q_m} \quad (8)$$

$$log q_e = \log K_f + \frac{1}{n} log C_e \quad (9)$$

Where q_e (mg g^{-1}) is the adsorbed amount at equilibrium, q_m (mg g^{-1}) is a constant related to the adsorption capacity, C_e(mg/mL) is the equilibrium concentration of the adsorbate, k (mg L^{-1}) is Langmuir constant related to the adsorption capacity, k_f (mg g^{-1}(L mg^{-1}) $^{1/n}$) is the Freundlich adsorption constant, and n is the intensity of the adsorption.

Photocatalytic Degradation Studies

The photocatalytic efficacy of Zn-MOF was investigated for the degradation of TC and Doxy in water using a photo-reactor equipped with two visible light lamps (40 W each, the distance between the flask and one lamp is 10 cm). Here, 5 mg of Zn-MOF was immersed into 50 mL of 10 ppm aqueous solution of TC or Doxy. In order to maintain the adsorption equilibrium, the solution was stirred for 2 h (700 rpm) in dark. Then the reaction mixture was exposed to visible light irradiation. Finally, 2 mL aliquots of TC or doxy solution were collected and centrifuged (1200 rpm) for 10 min and the residual concentrations were determined by UV-vis spectrophotometry.

Recyclability Studies

The recyclability studies were performed after adsorption and degradation experiments. The used Zn-MOF was immersed in the mixture of ethanol and acetone and was stirred for 3 h at 37 °C. Afterwards, the mixture was kept overnight. Finally, the MOF was collected through centrifuge and washed several times with ethanol before drying it at 80 ^{o}C.

Crystal Structure Analysis.

Single-crystal X-ray diffraction data of Zn-MOF was collected on an Agilent Supernova X-ray diffractometer equipped with a CCD detector at room temperature (296 K) using the source graphite-monochromatic Cu-Kα radiation (λ = 1.54184 Å). Data acquisition, reduction, and

absorption correction were performed by using the CrysAlis Pro program.[8] Absorption corrections were applied using SADABS.[9] Structures were solved by direct methods by using the SHELXS-2014 package[10] and refined with SHELXL-2014/6.[10] Calculations were performed using the WinGX System-Version 2014.1.[11] The hydrogen atoms attached to carbon and nitrogen atoms were inserted at geometrically calculated positions and included in the refinement using the riding-model approximation; Uiso(H) were defined as 1.2Ueq of the parent atoms for phenyl and 1.5Ueq of the parent atoms for the methyl groups and nitrogen atoms. Least square refinements with anisotropic thermal motion parameters for all the non-hydrogen atoms and isotropic ones for the remaining atoms were employed. Zn-MOF contains disordered methanol molecules which could not be modelled reliably. PLATON/SQUEEZE[12] was used to correct the data and in Zn-MOF potential volume of 1362 $Å^3$ was found with 266 electrons per unit cell worth of scattering, which indicate the presence of six DMF and two water molecules per unit cell. These disordered solvents were removed from the model and not included in the empirical formula. Crystallographic data is summarized in Table S1. CCDC (CCDC No = 2186058) contain the supplementary crystallographic data for this paper. These data can be obtained free of charge from The Cambridge Crystallographic Data Centre via www.ccdc.cam.ac.uk/data_request/cif.

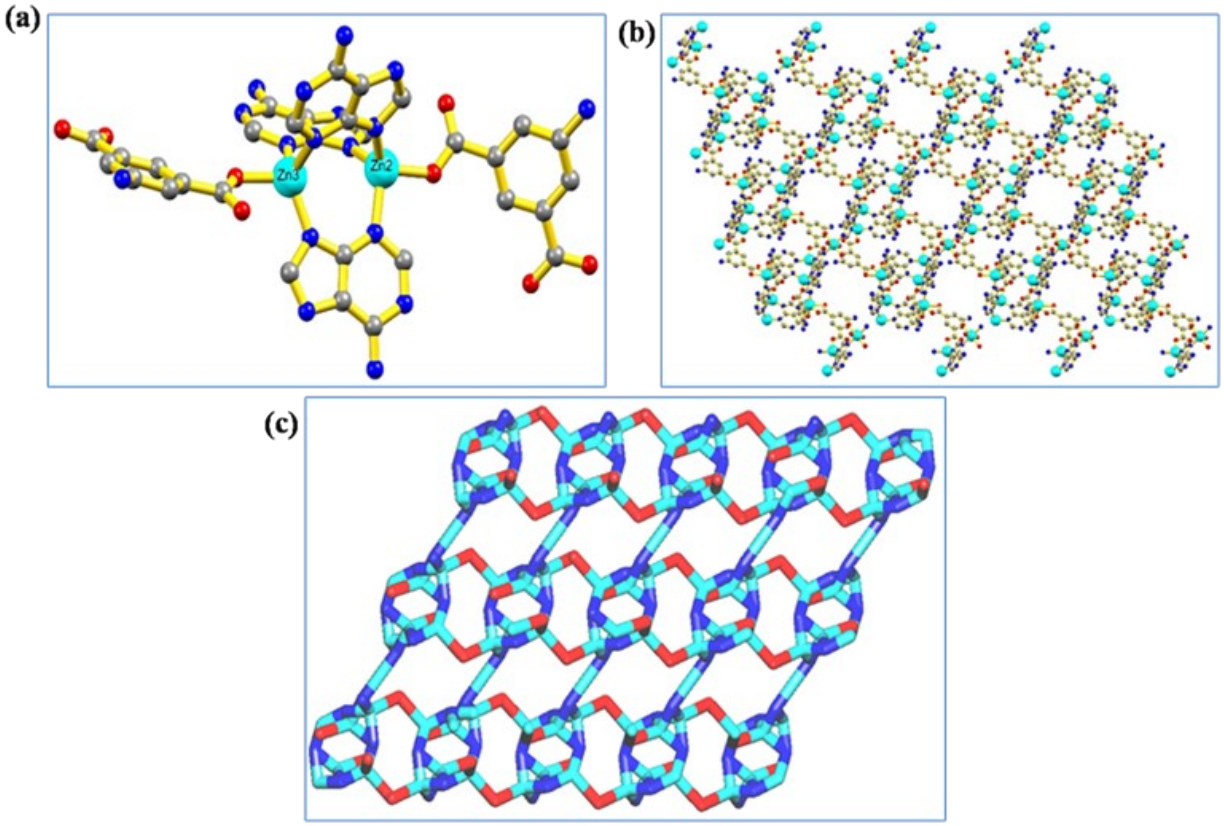

Fig. S1. (a) Dinuclear $[Zn_2(Ade)_3(COO)_2]$ secondary building unit (SBU) (b) Three-dimensional network of Zn-MOF presented in ball-stick model (c) Node-and-linker-type representation of Zn-MOF (the metal nodes are represented in cyan and the linker AIPA in red and Ade in blue color)

Table S1: Crystal data and structure refinement detail for Zn-MOF

Identification name	Zn-MOF
Formulae	$C_{62}H_{52}N_{34}O_{20}Zn_7$
Mol. wt.	2050.96
Crystal system	Triclinic
Space group	P-1
Temperature /K	296(2)
Wavelength /Å	0.71073
a /Å	12.0452(7)
b /Å	14.2181(7)
c /Å	18.0667(11)
α/°	104.144(5)
β/°	98.797(5)
γ/°	94.930(4)
V/ Å^3	2940.4(3)
Z	1
Density/Mgm^{-3}	1.158
Abs. Coeff. /mm^{-1}	2.095
F(000)	1032
Refl. collected	12765
Refl. unique	8227
Max. 2θ/°	66.915
Ranges (h, k, l)	-14<= h <=14 -12<= k <=16 -21<= l <=20
Complete to 2θ (%)	78.6
Data/Restraints/Parameters	8227/24/575
Goof (F^2)	1.030
R1 [I > 2s(I)]	0.0380
wR2 [I > 2s(I)]	0.1048
R1 [all data]	0.0440
wR2 [all data]	0.1108

Table S2: Selected bond distances (Å) and angles (°) for Zn-MOF

Zn-MOF	Zn1-O1 2.452(3); Zn1-O2 2.019(2); Zn1-O5 2.416(3); Zn1-O6 2.027(2); Zn1-N6 2.044(3); Zn1-N10 2.058(3); Zn2-O7 1.927(2); Zn2-N9 1.980(3); Zn2-N5 1.997(3); Zn2-N3 2.026(3); Zn3-O3 1.958(2); Zn3-N1 1.979(3); Zn3-N7 2.029(3); Zn3-N11 2.033(3); Zn4-N2 2.088(3); Zn4-O10 2.151(3); Zn4-O9 2.165(3). <O2-Zn1-O6 135.67(10); <O2-Zn1-N6 107.43(11); <O6-Zn1-N6 101.29(10); <O2-Zn1-N10 105.77(9); <O6-Zn1-N10 103.17(11); <N6-Zn1-N10 97.33(11); <O2-Zn1-O5 89.44(10); <O6-Zn1-O5 58.02(9); <N6-Zn1-O5 159.28(9); <N10-Zn1-O5 89.25(11); <O2-Zn1-O1 57.56(8); <O6-Zn1-O1 88.31(10); <N6-Zn1-O1 93.11(11); <N10-Zn1-O1 162.58(9); <O5-Zn1-O1 85.79(12); <O7-Zn2-N9 111.23(12); <O7-Zn2-N5 112.11(11); <N9-Zn2-N5 107.65(11); <O7-Zn2-N3 95.47(11); <N9-Zn2-N3 114.05(12); <N5-Zn2-N3 116.02(11);<O3-Zn3-N1 111.27(11); <O3-Zn3-N7 110.25(11); <N1-Zn3-N7 112.90(12); <O3-Zn3-N11 94.40(10); <N1-Zn3-N11 115.64(11); <N7-Zn3-N11 110.94(12); <N2-Zn4-N2 180.0; <N2-Zn4-O10 91.75(12); <N2-Zn4-O10 88.25(12); <N2-Zn4-O10 88.26(12); <N2-Zn4-O10 91.75(12); <O10-Zn4-O10 180.0; <N2-Zn4-O9 90.32(11); <N2-Zn4-O9 89.68(11); <O10-Zn4-O9 88.15(15); <O10-Zn4-O9 91.85(15); <N2-Zn4-O9 89.69(11); <N2-Zn4-O9 90.31(11); <O10-Zn4-O9 91.85(15); <O10- Zn4-O9 88.15(15); <O9-Zn4-O9 180.0.

Table S3. Hydrogen bond geometry (Å, °) in Zn-MOF

	D-H···A	D···H (Å)	H···A (Å)	D···A (Å)	<D−H···A(°)
Zn-MOF	N12-H12A···N15	0.86	2.24	3.049(4)	157.3
	N8-H8A···N13	0.86	2.27	3.015(4)	145.3
	N4-H4A···N14	0.86	2.31	3.078(4)	148.3
	N17A-H17B···N15	0.86	2.63	3.245(9)	129.4
	N17A-H17B···N15	0.86	2.64	3.380(9)	144.9
	N17B-H17C···N15	0.86	2.47	3.287(13)	159.3
	N12-H12B···O2	0.86	1.99	2.842(3)	172.3
	N8-H8B···O6	0.86	2.21	2.987(4)	150.4
	N16-H16B···O4	0.86	2.17	2.974(4)	155.2
	N4-H4B···O9	0.86	2.28	3.059(5)	151.3
	N4-H4B···O10	0.86	2.58	3.100(5)	120.0
	O9-H9A···N16	0.96	2.33	3.022(5)	128.2
	C20-H20···O4	0.93	2.42	3.208(4)	142.1
	C28-H28···O7	0.93	2.29	2.931(4)	125.6
	C39-H39···O8	0.93	2.37	3.153(4)	142.2
	C43-H43···O4	0.93	2.54	3.285(5)	136.9
	C49-H49···O3	0.93	2.20	2.858(4)	127.0

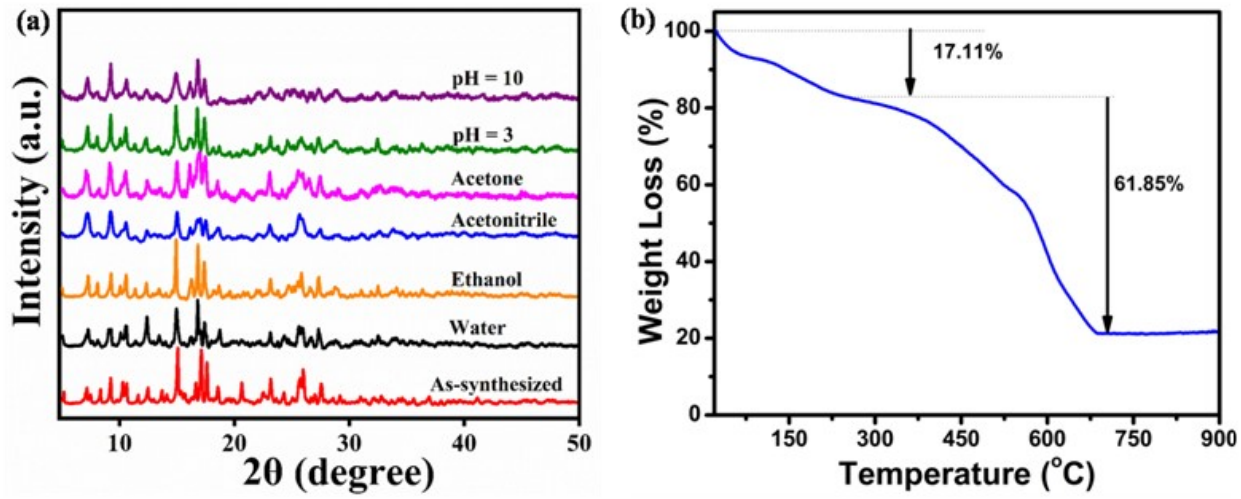

Fig. S2. (a) PXRD patterns of Zn-MOF in different solvents and pH medium (b) Thermogravimetric analysis of Zn-MOF

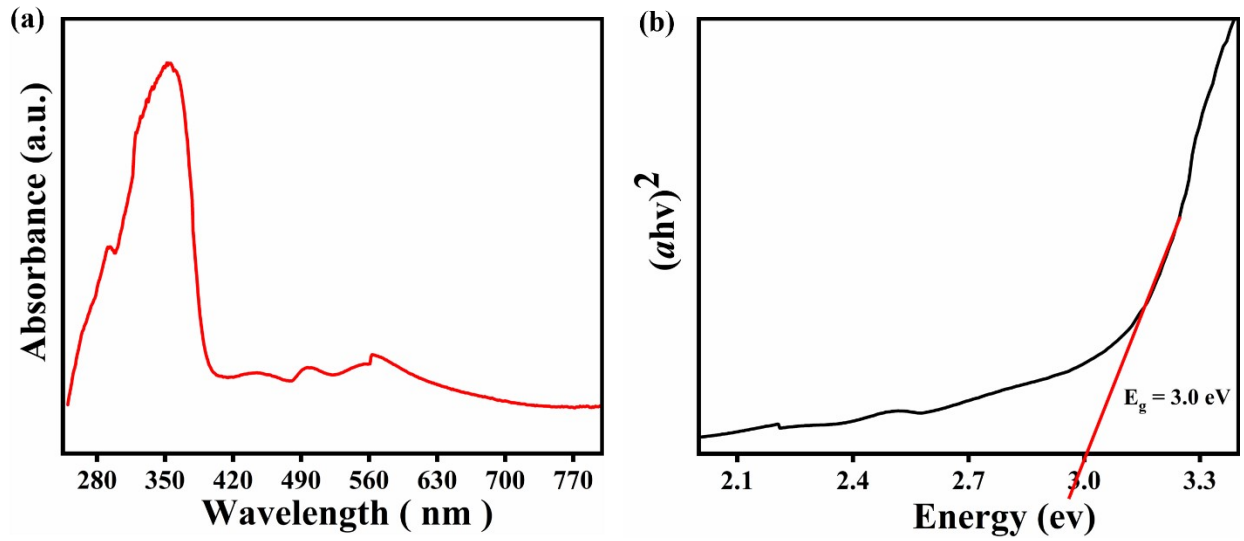

Fig. S3. (a) UV-vis diffuse reflectance spectroscopy of Zn-MOF (b) Tauc plot for the calculation of band gap of Zn-MOF

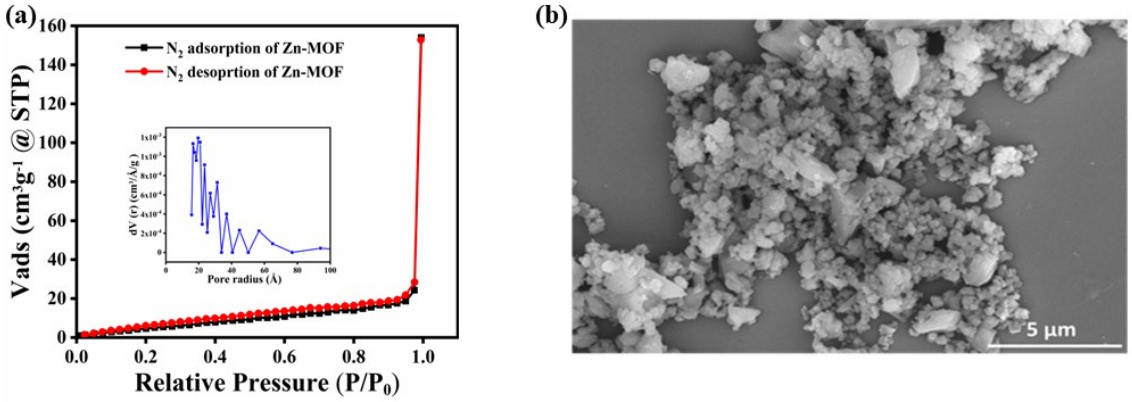

Fig. S4. (a) N_2 adsorption/desorption isotherms (inset shows pore size distribution for Zn-MOF evaluated by using N_2 adsorption data measured at 77 K) (b) SEM image of Zn-MOF

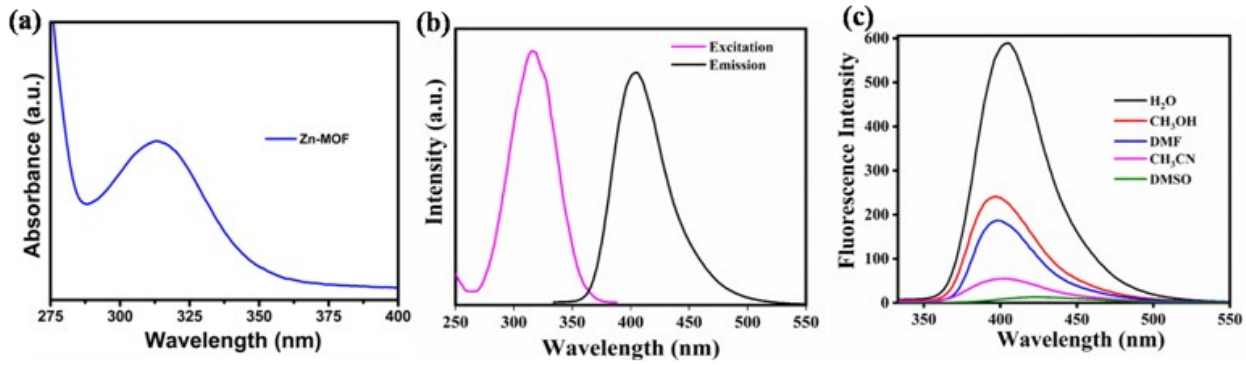

Fig. S5. (a) UV-vis absorption spectrum of Zn-MOF (b) Normalized excitation and emission spectra of Zn-MOF (c) Fluorescence emission profile of Zn-MOF in different solvent systems

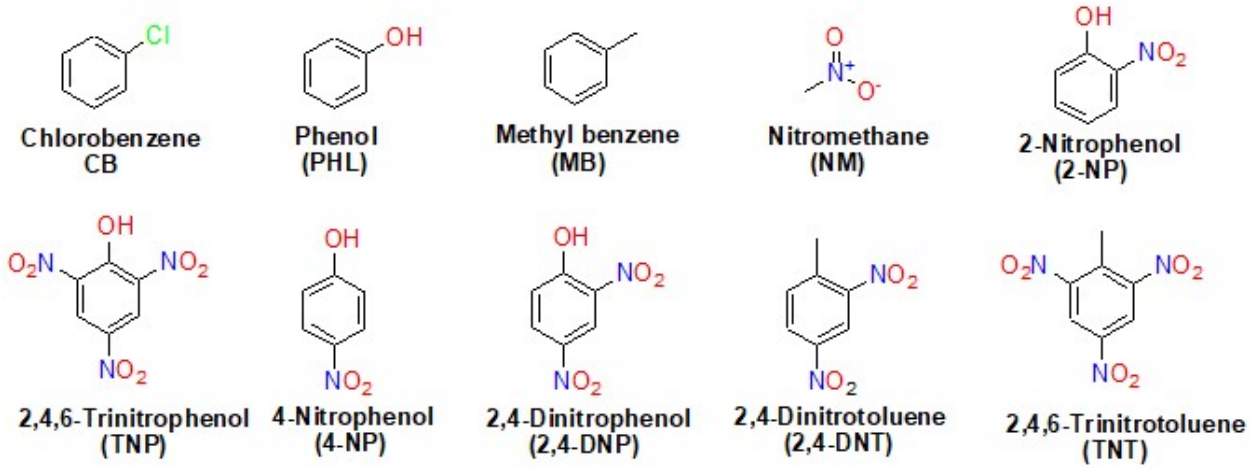

Fig. S6. Structure of different explosives used for the studies

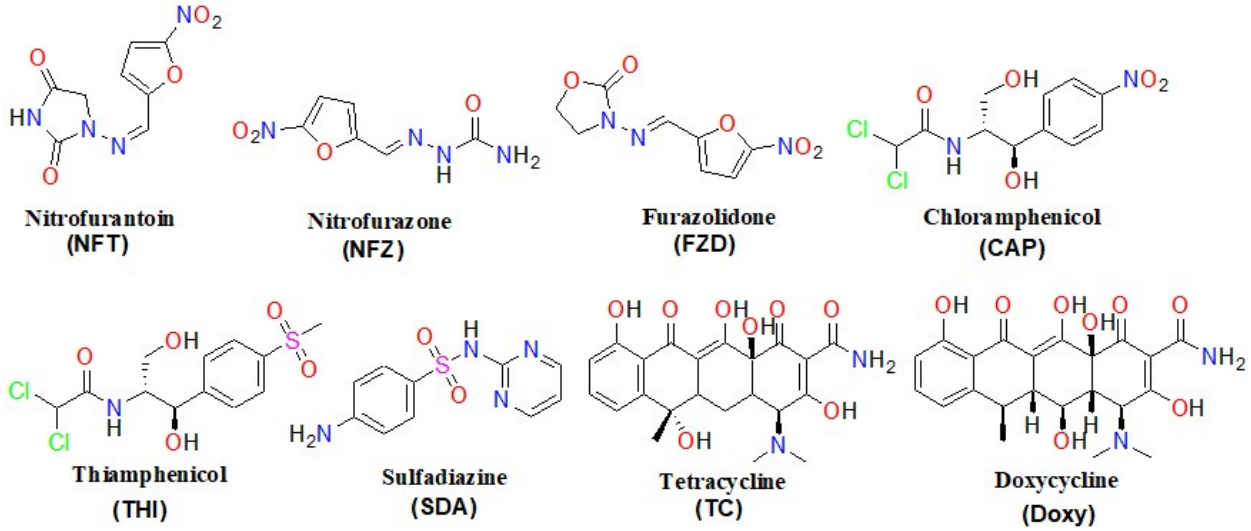

Fig. S7. Structure of different antibiotics used for the studies

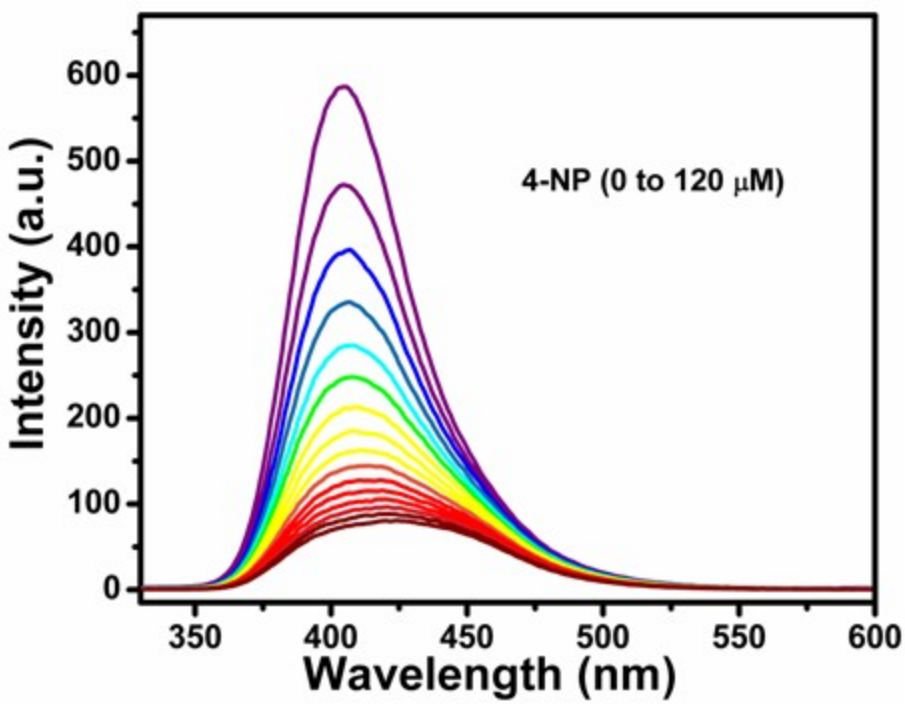

Fig. S8. Reduction in emission intensity of Zn-MOF dispersed in water upon incremental addition of 4-NP (1 mM solution)

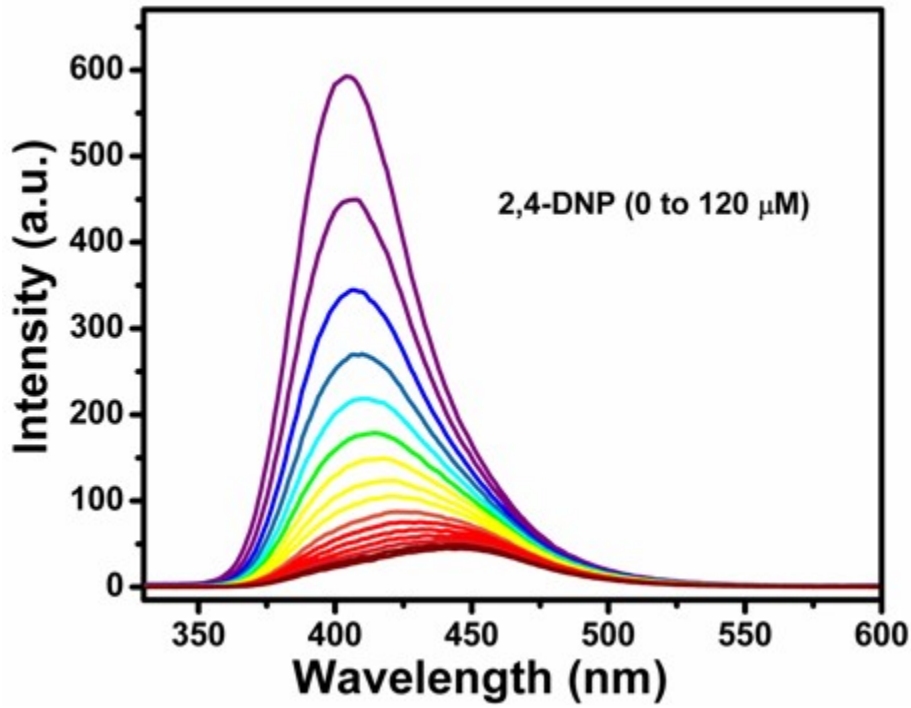

Fig. S9. Reduction in emission intensity of Zn-MOF dispersed in water upon incremental addition of 2,4-DNP (1 mM solution)

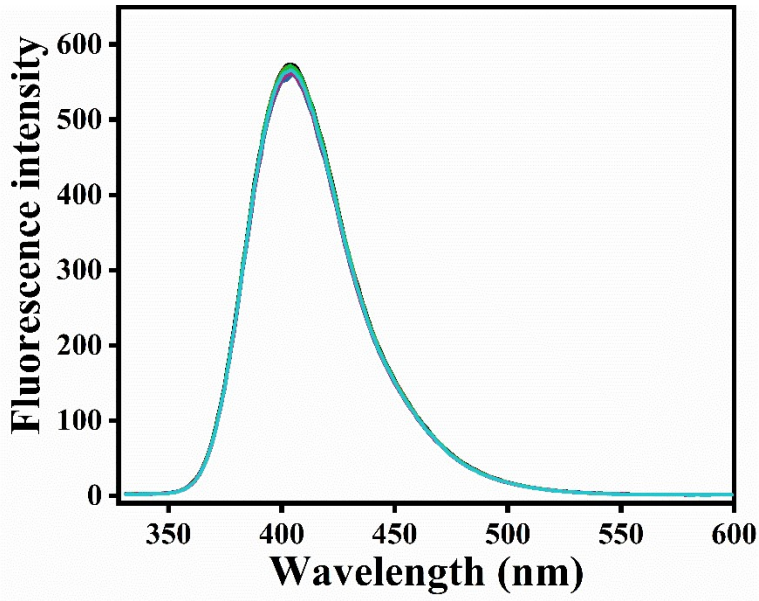

Fig. S10. Reduction in emission intensity of Zn-MOF dispersed in water upon incremental addition of TNT (1 mM solution)

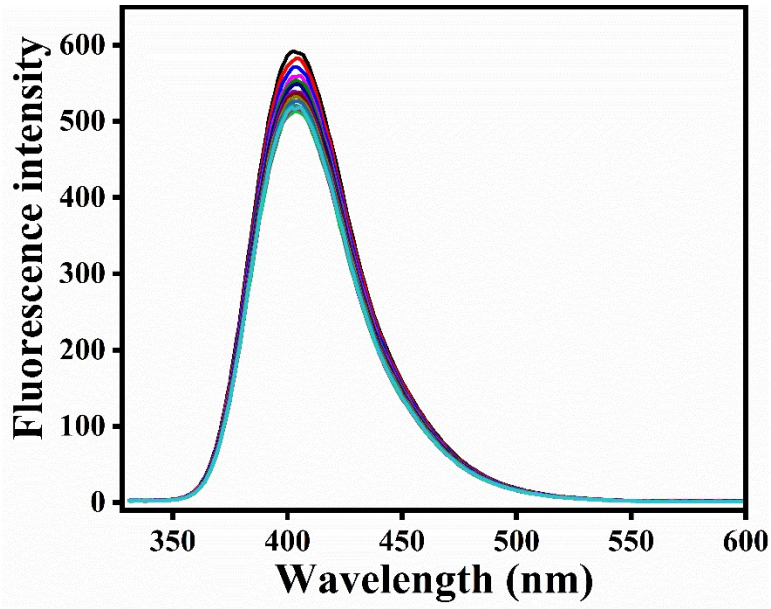

Fig. S11. Reduction in emission intensity of Zn-MOF dispersed in water upon incremental addition of DNT (1 mM solution)

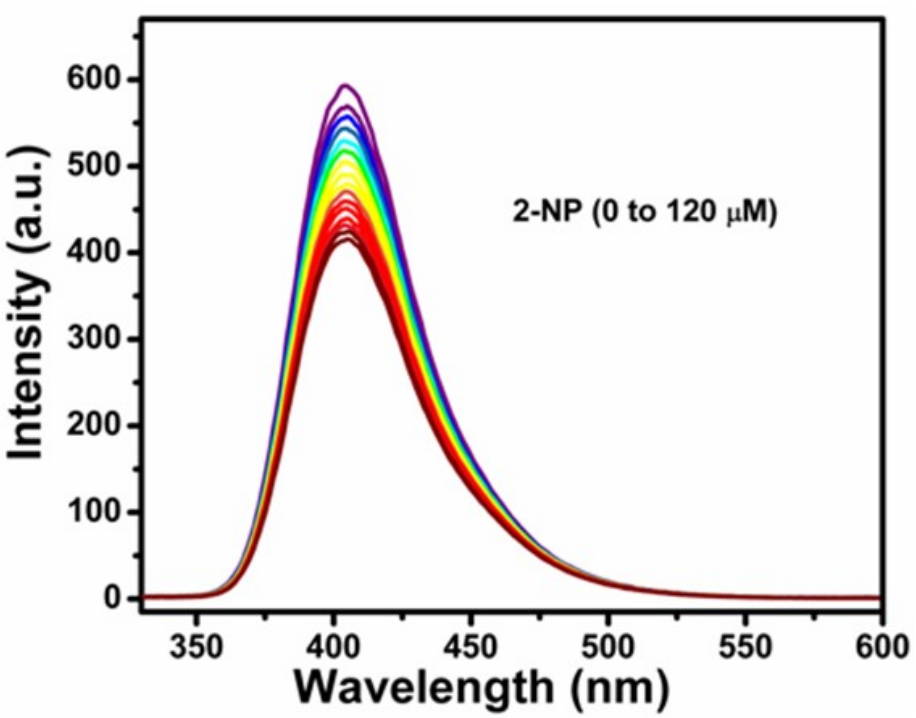

Fig. S12. Reduction in emission intensity of Zn-MOF dispersed in water upon incremental addition of 2-NP (1 mM solution)

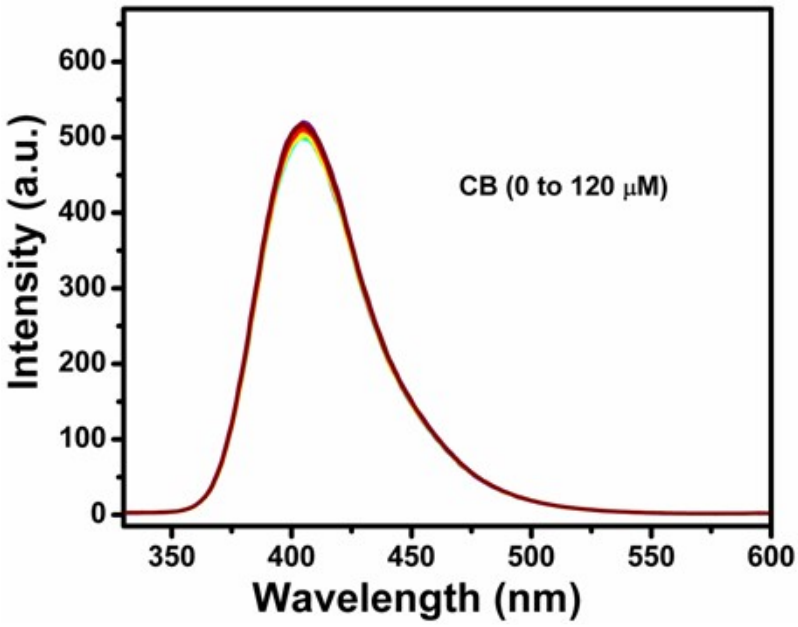

Fig. S13. Reduction in emission intensity of Zn-MOF dispersed in water upon incremental addition of CB (1 mM solution)

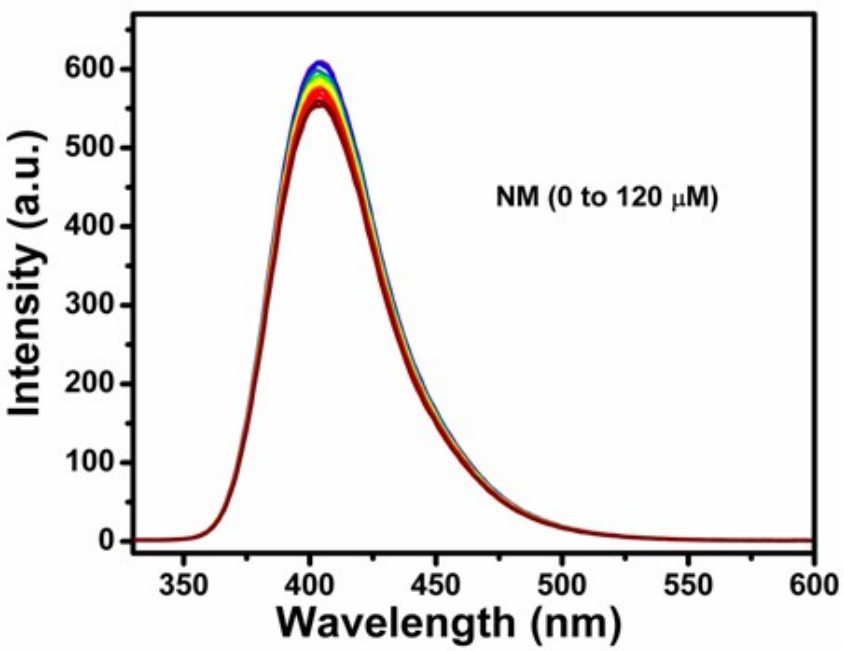

Fig. S14. Reduction in emission intensity of Zn-MOF dispersed in water upon incremental addition of NM (1 mM solution)

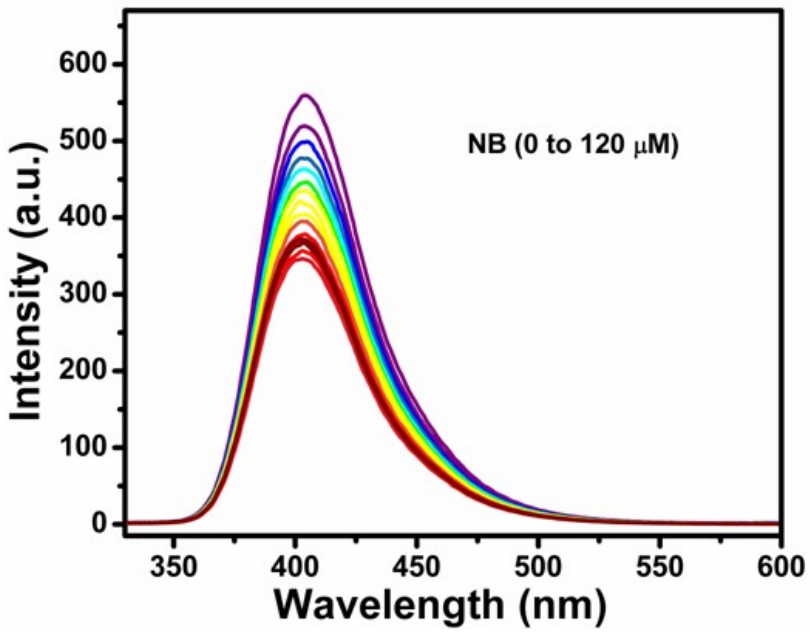

Fig. S15. Reduction in emission intensity of Zn-MOF dispersed in water upon incremental addition of NB (1 mM solution)

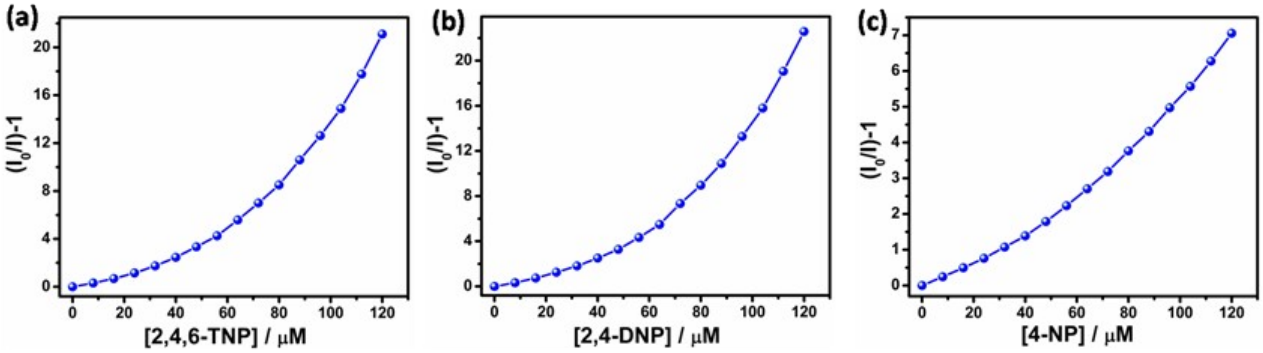

Fig. S16. Stern−Volmer plot of $(I_0/I) - 1$ versus increasing concentration of (a) 2,4,6-TNP (b) 2,4-DNP (c) 4-NP

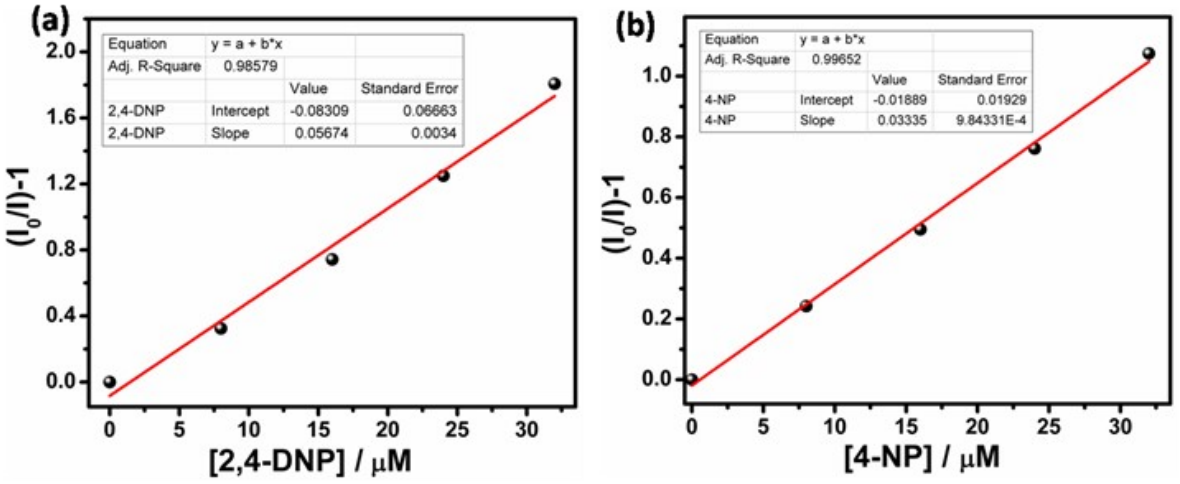

Fig. S17. Linear part of Stern−Volmer plot for Zn-MOF in the presence of (a) 2,4-DNP and (b) 4-NP

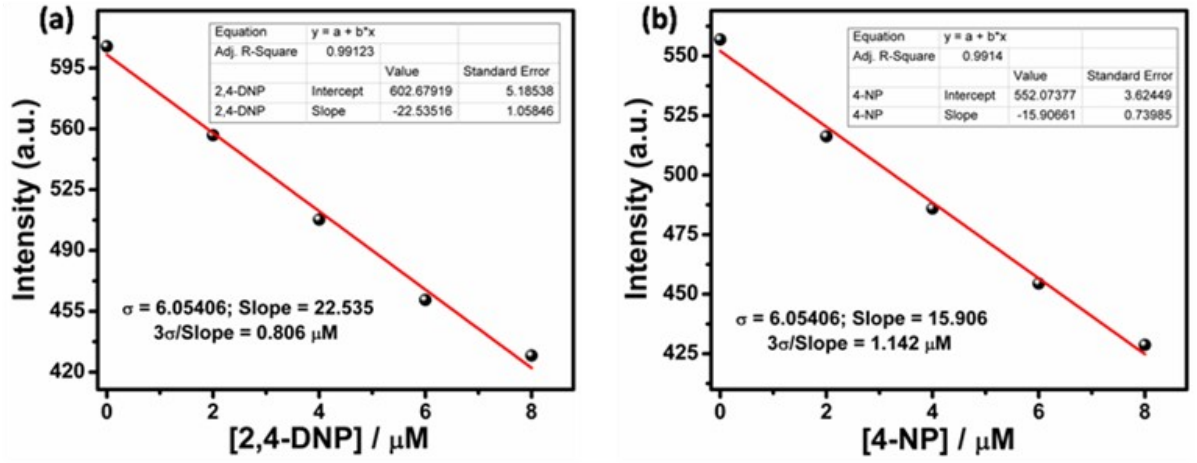

Fig. S18. Linear region of fluorescence intensity of Zn-MOF in water versus concentration of (a) 2,4-DNP and (b) 4-NP

Table S4. Stern-Volmer constant (K_{sv}) and LOD of different explosives with Zn-MOF

S. No.	Explosives	K_{sv} (M^{-1})	LOD (μM)
1.	2,4,6-TNP	0.5406×10^5	0.979
2.	2,4-DNP	0.567×10^5	0.806
3.	4-NP	0.333×10^5	1.142

Table S5. Comparison of K_{sv} value and detection limit of Zn-MOF for the detection of TNP, 2,4 -DNP and 4- NP with other reported MOFs

S.No.	MOF	Analyte	Media	$K_{sv}(M^{-1})$	LOD	Ref.
1.	AHU-TW1	TNP	DMF	1.44×10^4	4.05μM	[13]
2.	$[Zn_2(NO_3)_2(4,4'\text{-}bpy)_2(TBA)]$	TNP	Ethanol	4.28×10^4	6.02 μM	[14].
3.	$\{[Zn(L)(H_2O)_2]\cdot H_2O\}n$	TNP	Water	9.77×10^4	0.63μM	[15]
4.	$[Zn(OBA)(H_2DPT)0.5]n\cdot DMF$	TNP	Water	182663	8.1 μM	[16]
5.	$[Zn_3(TIAB)_2(IMDC)_2]\cdot(NO_3)_2\cdot(DMF)_2\cdot(H2O)_2$	TNP	DMSO	56760	0.78 μM	[17]
6.	$Ti_6(\mu_3\text{-}O)_6(\mu_2\text{-}OH)_6(BTB)_2(DMF)_2$	TNP	Ethanol	2.266×10^4	2.37 μM	[18]
7.	H_8L-Ti-MOF	TNP	Water	8.7×10^5	3.6 μM	[19]
8.	$[Zn_2(NH_2BDC)_2(dpNDI)]n$	TNP	Water	7.3×10^4	0.3ppm	[20]
9.	$\{[Zn_2(Py_2TTz)_2(BDC)_2]\cdot 2(DMF)\cdot 0.5\ (H_2O)\}n$	TNP	Water	3.257×10^4	0.93 μM	[21]
10.	**Zn-MOF**	**TNP**	**Water**	**0.5406×10^5**	**0.979μM**	**This work**
11.	$[Cd(TTPBA4)_2(OH)_2\cdot H_2O]n$	2,4 - DNP	Water	4.1×10^4	1.4ppm	[22]
12.	[Cd(ppvppa)(1,4-NDC)]n	2,4 - DNP	Water	118	-	[23]
13.	$[Tb(L^{2-})(HL^{-})(H_2O)_2]n$	2,4 - DNP	Ethanol	7.75×10^3	16.2 μM	[24]
14.	FJI-C8	2,4 - DNP	DMF	5.11×10^4	2.866 μM	[25]

15.	JLU-MOF201-Y	2,4 - DNP	DMF	3.63×10^4	0.46 μM	[26]	
16.	**Zn-MOF**	**2,4-DNP**	**Water**	**0.567×10^5**	**0.806μM**	**This work**	
17.	[Cd(TTPBA-4)$_2$(OH)$_2$·H_2O]n	4 - NP	Water	$2.24\ 10^4$	2.2 ppm	[22]	
18.	JLU-MOF201-Tb	4 - NP	DMF	1.89×10^4	1.01 μM	[26]	
19.	{[$Eu_2L_3(H_2O)_5]_2$·3DMF}n	4 - NP	Water	3.8×10^4	1.6 μM	[27]	
20.	[Zn(L)(H_2O)]·H_2O	4 - NP	Water	1.25×10^4	3.74 μM	[28]	
21.	{[Eu_2(NSBPDC)$_3$(H_2O)$_4$]·x(H_2O)n	4 - NP	Ethanol	7.9248×10	9.3537 μM	[29]	
22.	**Zn-MOF**	**4 - NP**	**Water**	**0.333×10^5**	**1.142μM**	**This work**	

Antibiotics:

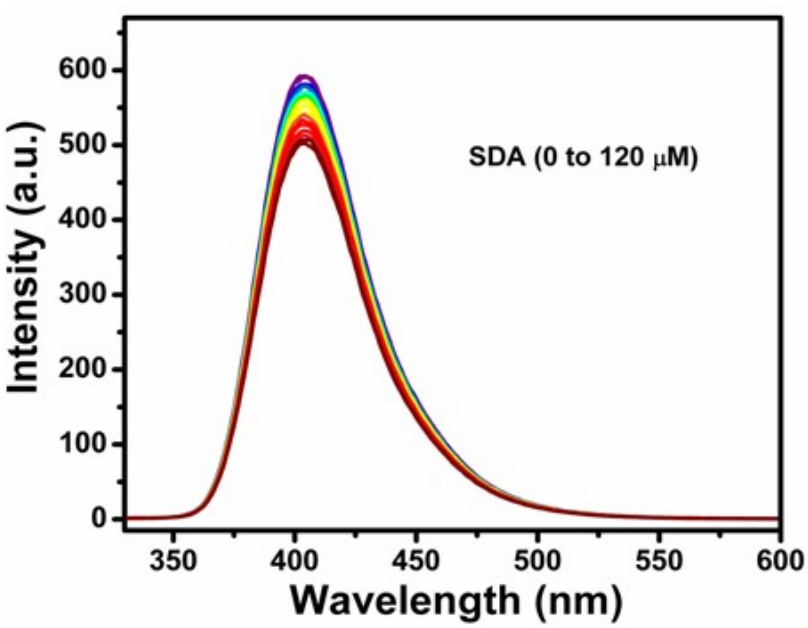

Fig. S19. Reduction in emission intensity of Zn-MOF dispersed in water upon incremental addition of SDA (1 mM solution)

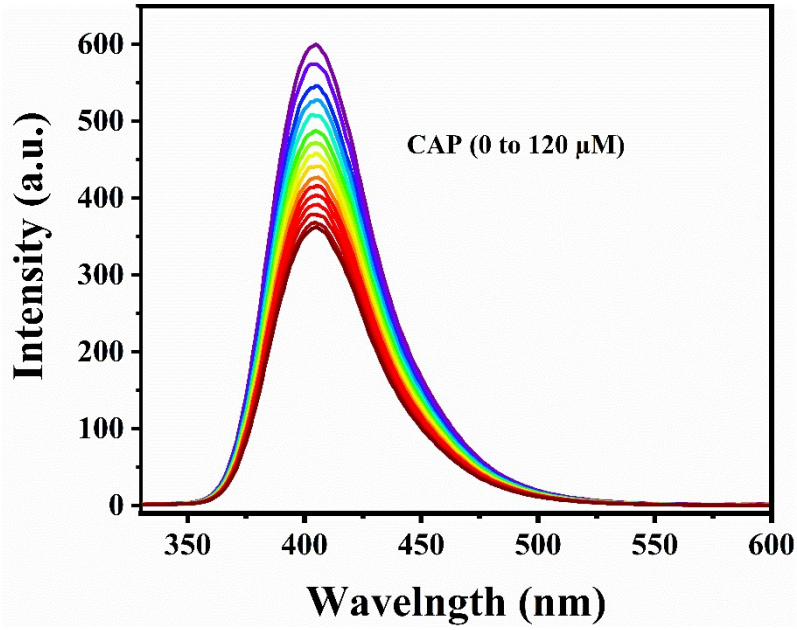

Fig. S20. Reduction in emission intensity of Zn-MOF dispersed in water upon incremental addition of CAP (1 mM solution)

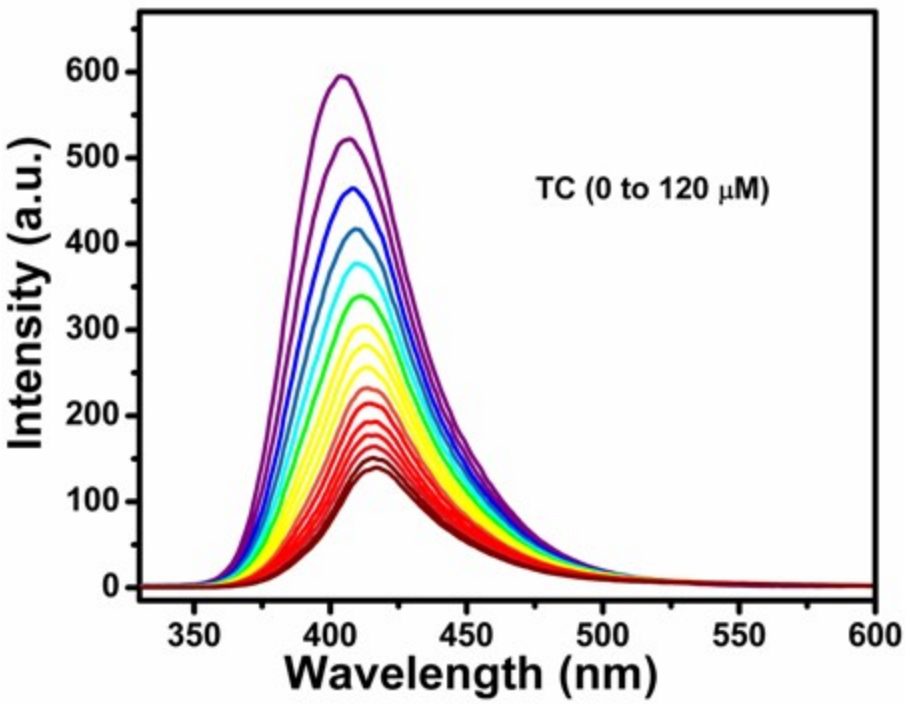

Fig. S21. Reduction in emission intensity of Zn-MOF dispersed in water upon incremental addition of TC (1 mM solution).

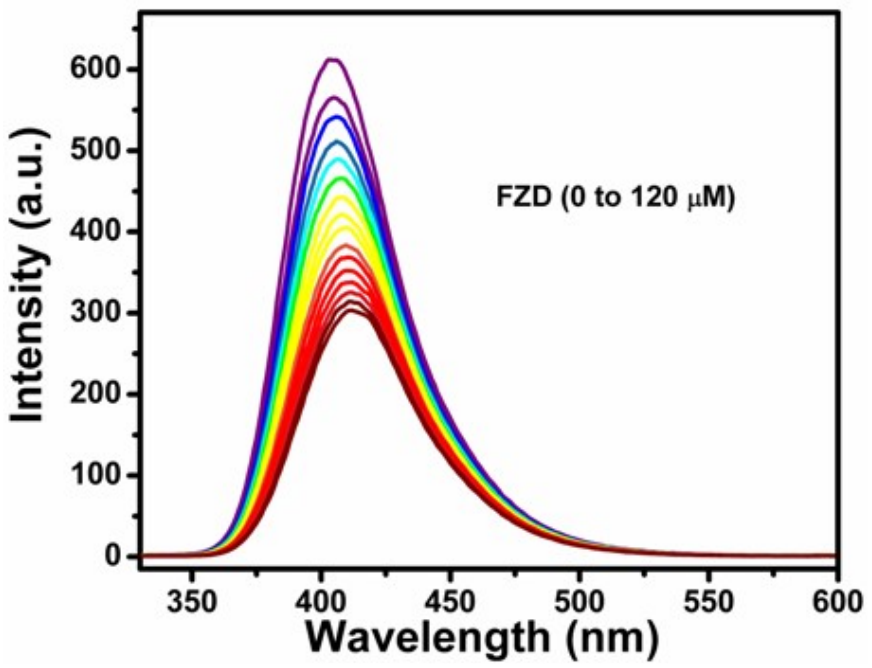

Fig. S22. Reduction in emission intensity of Zn-MOF dispersed in water upon incremental addition of FZD (1 mM solution).

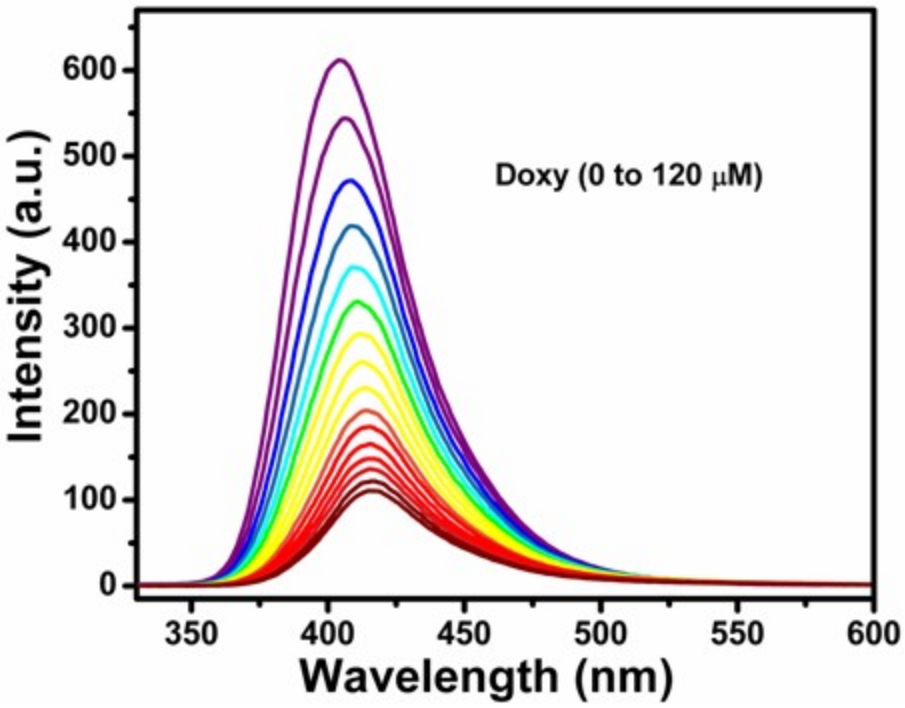

Fig. S23. Reduction in emission intensity of Zn-MOF dispersed in water upon incremental addition of Doxy (1 mM solution)

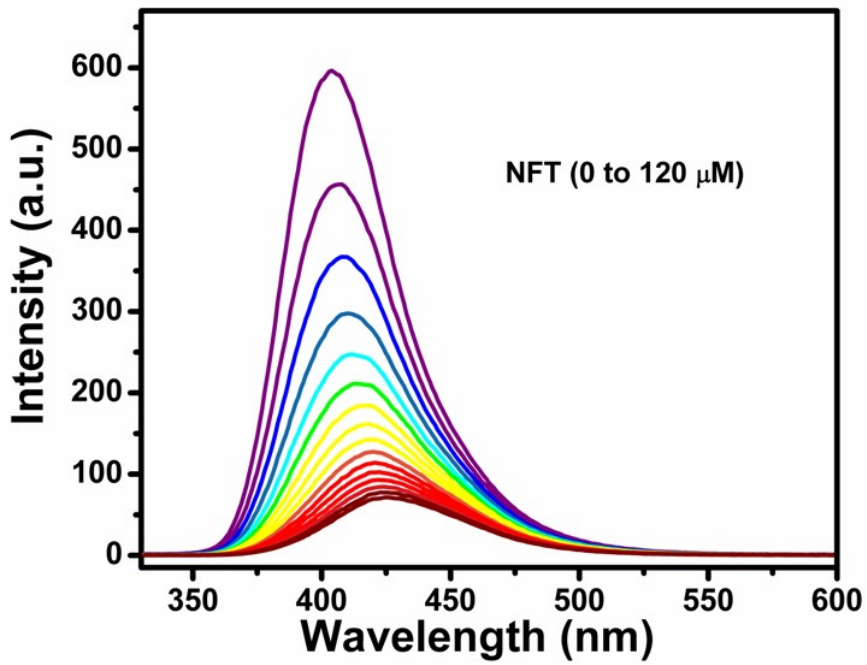

Fig. S24. Reduction in emission intensity of Zn-MOF dispersed in water upon incremental addition of NFT (1 mM solution)

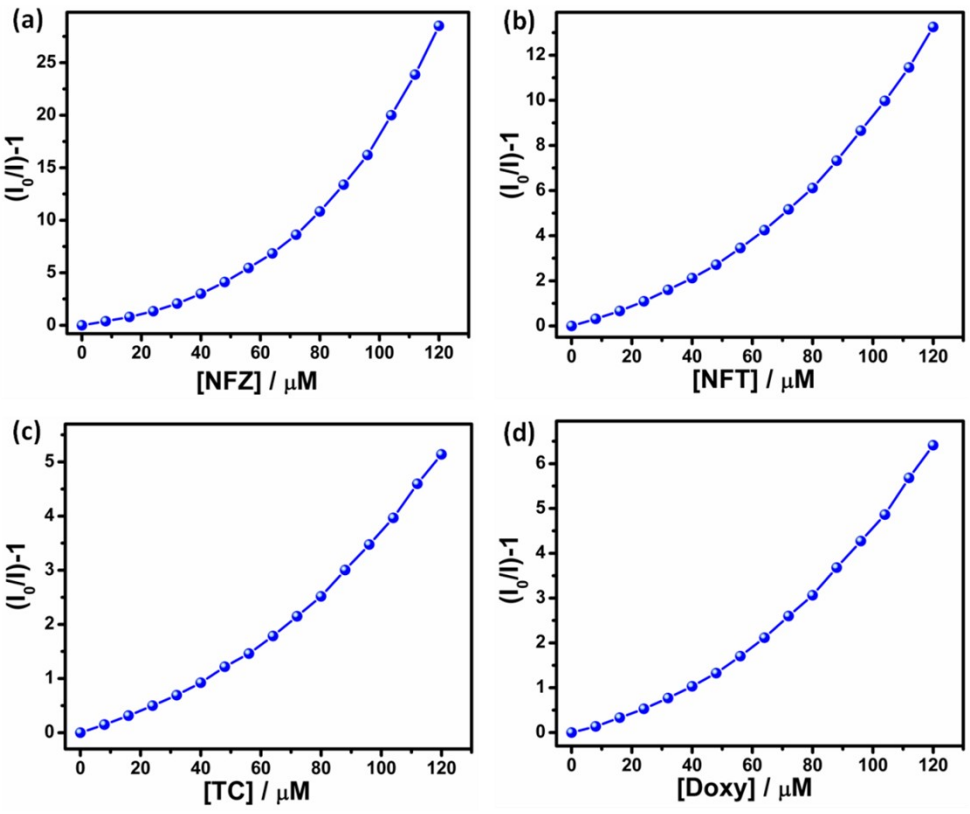

Fig. S25. Stern−Volmer plot of $(I_0/I) - 1$ versus increasing concentration of (a) NFZ, (b) NFT, (c) TC and (d) Doxy

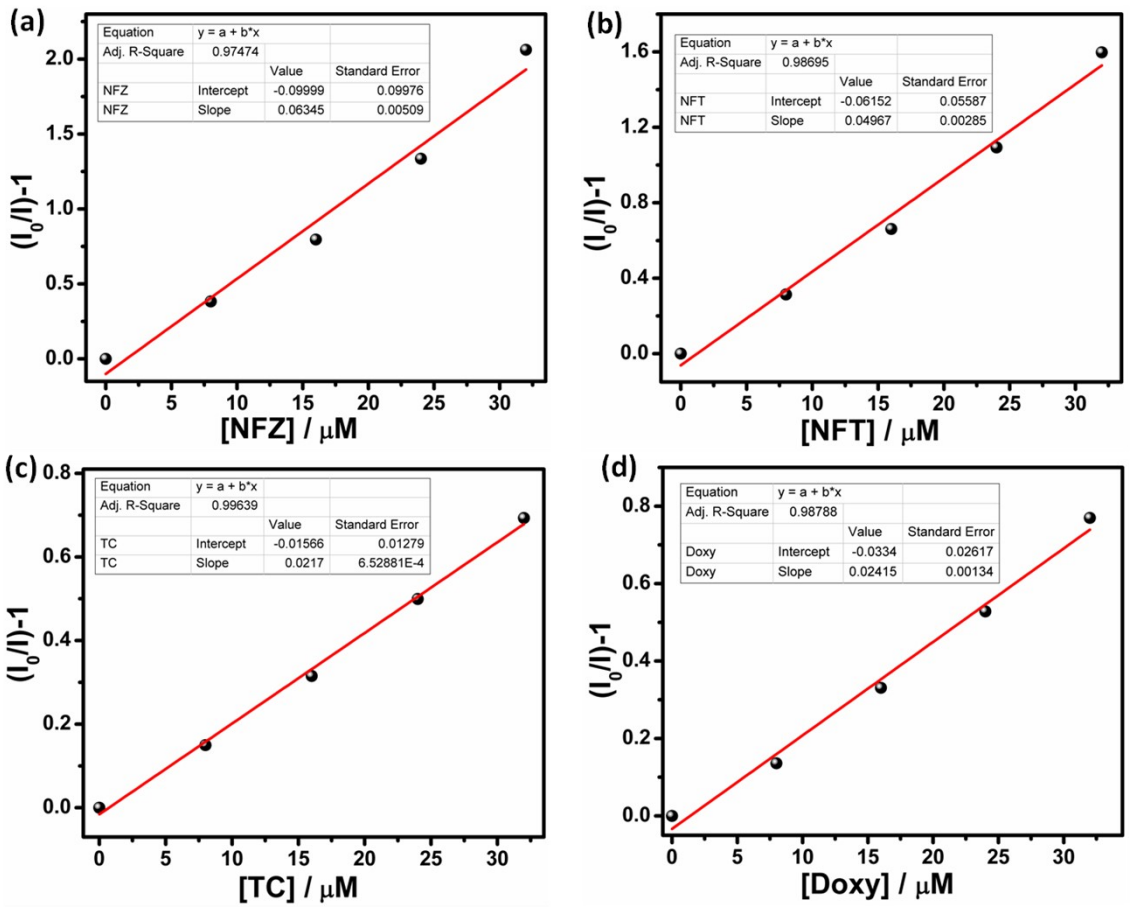

Fig. S26. Linear part of Stern−Volmer plot of Zn-MOF in the presence of (a) NFZ, (b) NFT, (c) TC and (d) Doxy

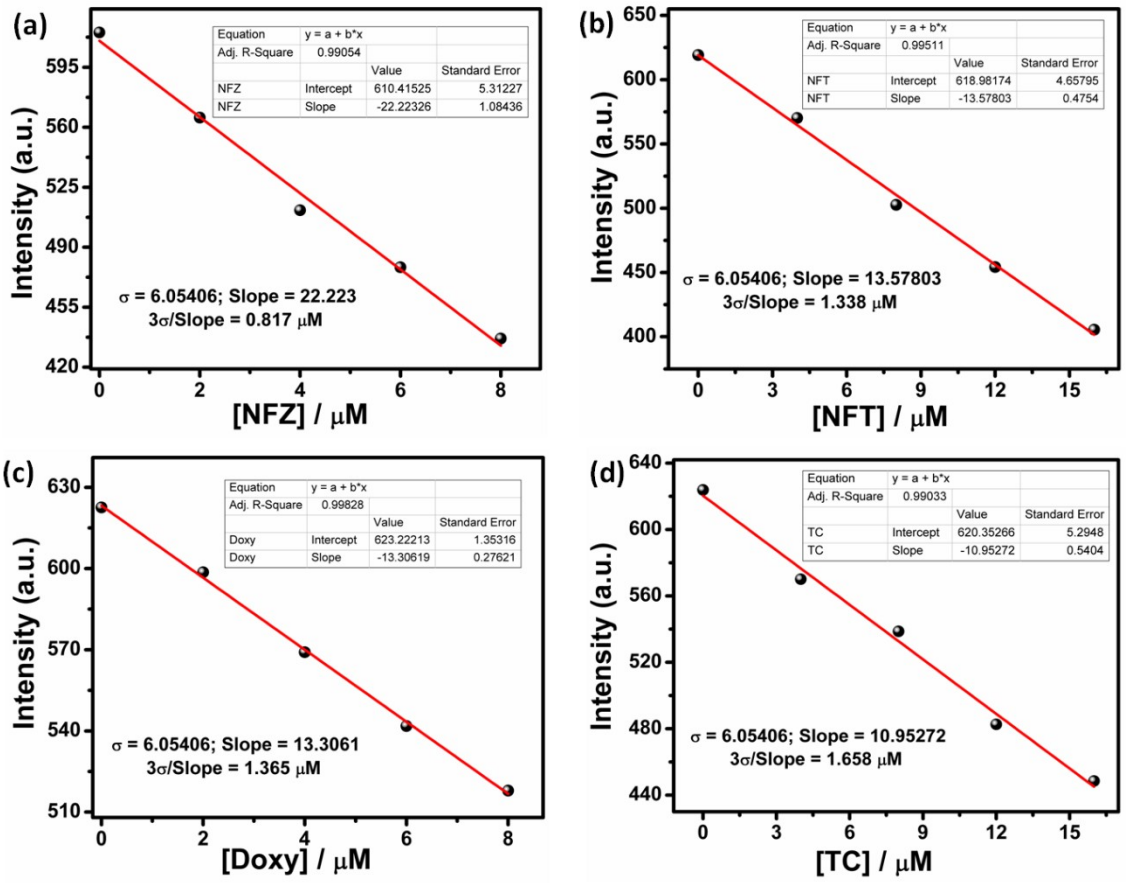

Fig. S27. Linear region of fluorescence intensity of Zn-MOF in water versus concentration of (a) NFZ (b) NFT (c) Doxy and (d) TC

Table S6. Stern-Volmer constant (K_{sv}) and LOD of different antibiotics-based analytes using Zn-MOF

S. No.	Antibiotics	K_{sv} (M^{-1})	LOD (μM)
1.	NFT	0.496×10^5	1.338
2.	NFZ	0.634×10^5	0.817
3.	TC	0.217×10^5	1.365
4.	Doxy	0.245×10^5	1.658

Table S7. Comparison of K_{sv} value and detection limit of Zn-MOF for the detection of NFZ and NFT with other reported MOFs

S.No.	MOFs	Analyte	Media	K_{sv} (M^{-1})	LOD	Ref.
1.	$[NaCd_2(L)(BDC)_{2.5}].9H_2O$	NFZ	DMF	5.06×10^4	162 ppb	30
		NFT	DMF	3.57×10^4	-	
2.	$[Cd_2(Py_2TTz)_2(BDC)]$	NFZ	Water	4.538×10^4	0.85 µM	21
	$Zn_2(Py2TTz)_2(BDC)_2]\cdot$	NFZ	Water	1.724×10^4	0.91 µM	
3.	$\{[Zn_3(cbbi)_2(bpe)(H_2O)_6]\cdot 2H_2O\}n$	NFT	-	13190	0.53 ppm	31
		NFZ	-	11352	0.72 ppm	
	$\{[Zn_4(OH)_2(cbbi)_2(bpee)(H_2O)_4]\cdot 4H_2O\}n$	NFT	-	54348	0.15 ppm	
		NFZ	-	37448	0.22 ppm	
4.	$\{(Me_2NH_2)[In(BCP)]\cdot 2.5DEF\}n$	NFZ	Water	6.38×10^4	0.2ppm	32
5.	$\{[Eu_2Na(Hpddb)(pddb)_2(CH_3COO)_2]\cdot_{2\cdot5}(DMA)n$	NFZ	DMF	4.93×10^4	0.64 µM	33
		NFT	DMF	4.42×10^4	0.68 µM	
6.	HNU-52	NFT	DMF	-	0.92 µM	34
		NFZ	DMF	-	0.72 µM	
7.	$[Cd_2(L)(bpda)_2]\cdot 3DMF\cdot H_2O$	NFZ	DMF	3.1×10^4	252 ppb	35
		NFT	DMF	2.2×10^4	465 ppb	

8.	$[Cd(tib)_2](NO_2)_2 \cdot 0.5DMA \cdot H_2O\}_n$	NFZ	Water	2.95×10^4	0.110 ppm	36
		NFT	Water	4.67×10^4	0.227 ppm	
9.	**Zn-MOF**	**NFZ**	**Water**	**0.634×10^5**	**0.817 µM**	**This work**
		NFT	**Water**	**0.496×10^5**	**1.338 µM**	

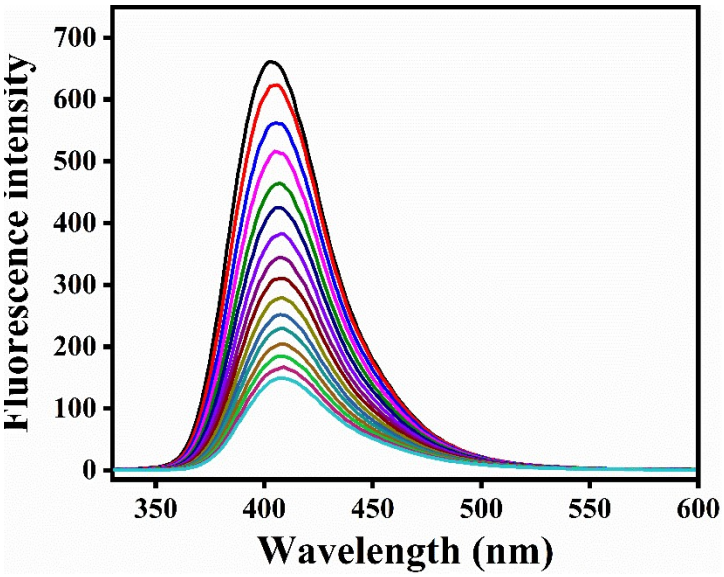

Fig. S28. Reduction in emission intensity of Zn-MOF dispersed in water upon incremental addition of TC in the presence of 10 equiv. $Na_2S_2O_4$

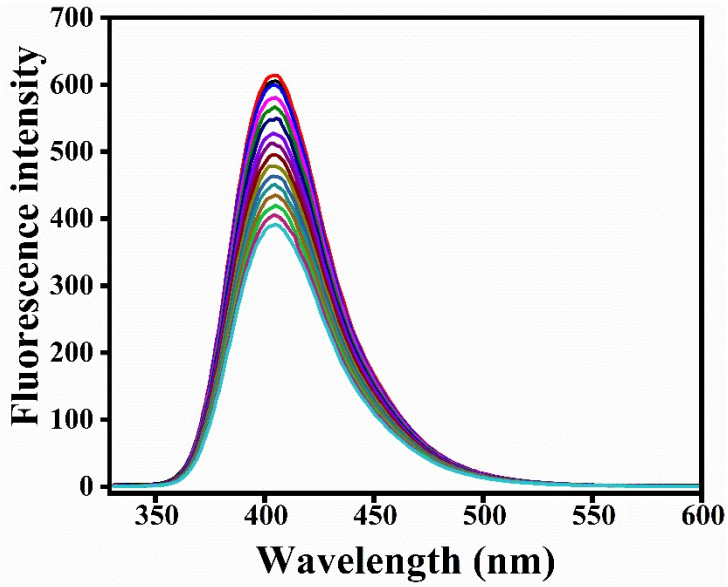

Fig. S29. Reduction in emission intensity of Zn-MOF dispersed in water upon incremental addition of NFT in the presence of 10 equiv. $Na_2S_2O_4$

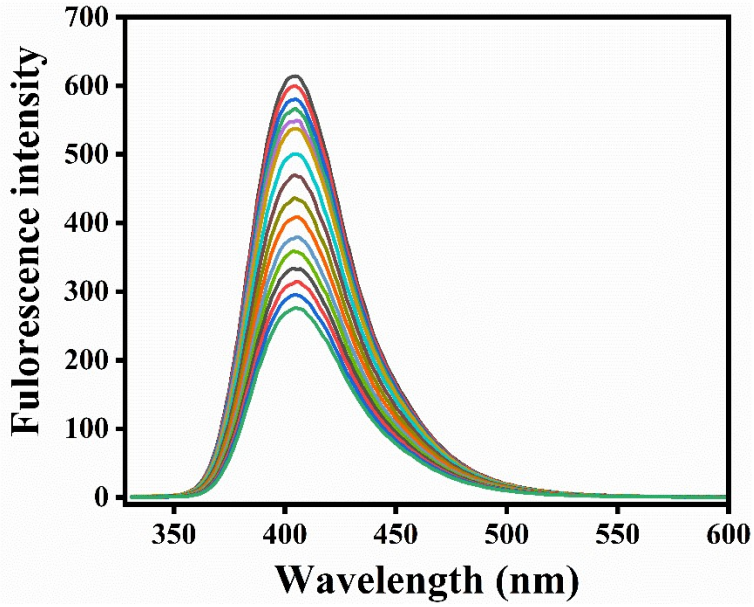

Fig. S30. Reduction in emission intensity of Zn-MOF dispersed in water upon incremental addition of NFZ in the presence of 10 equiv. $Na_2S_2O_4$

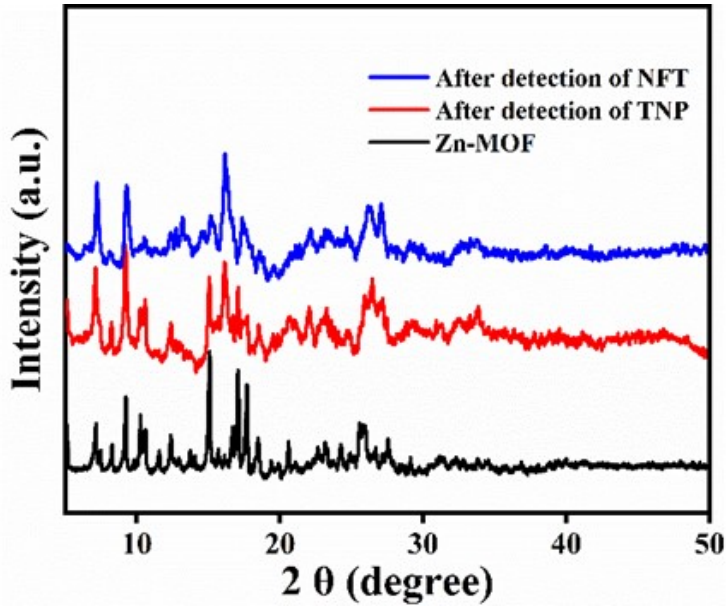

Fig. S31. PXRD patterns of Zn-MOF before and after detection of NFT and TNP

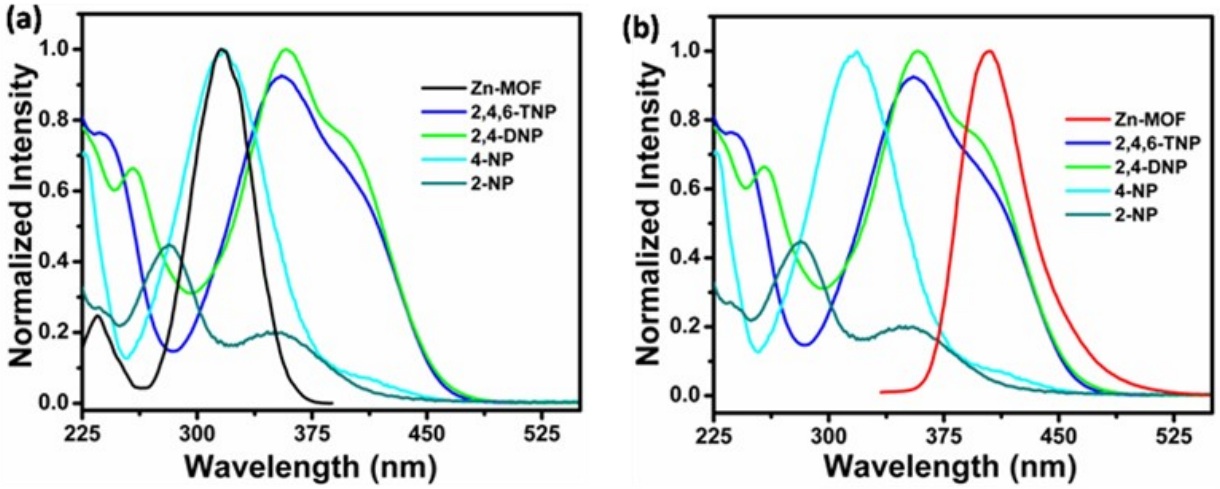

Fig. S32. Spectral overlap between normalized UV-vis spectra of nitroaromatic explosives and (a) excitation spectrum of Zn-MOF (b) emission spectrum of Zn-MOF

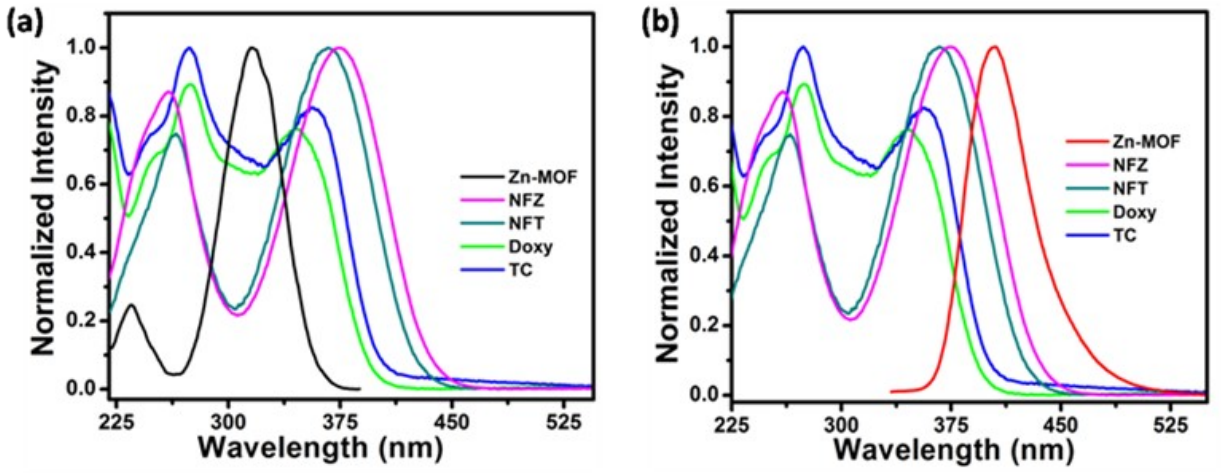

Fig S33. Spectral overlap between normalized UV-vis spectra of antibiotics and (a) excitation spectrum of Zn-MOF (b) emission spectrum of Zn-MOF

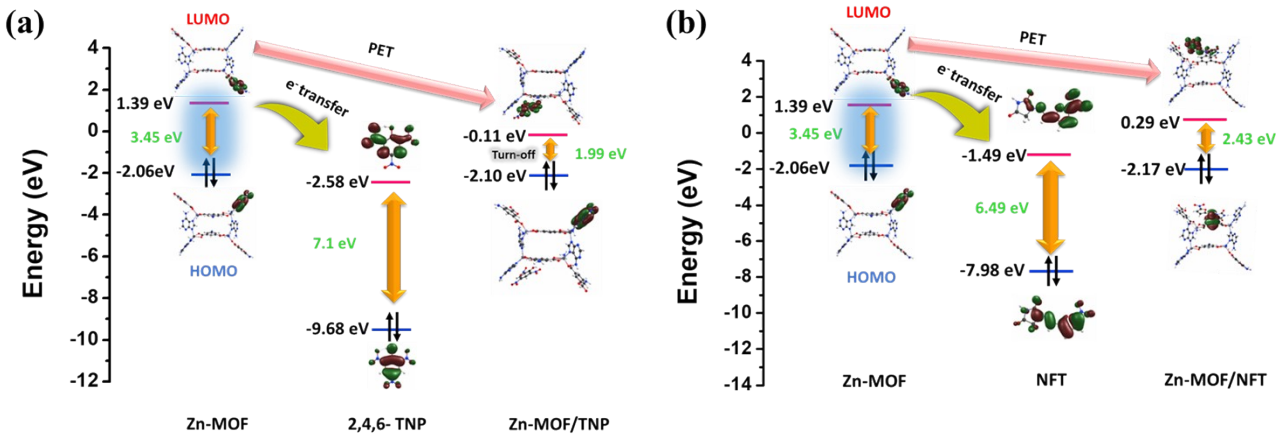

Fig. S34. HOMO-LUMO for Zn-MOF, (a) TNP and (b) NFT and the redistribution of HOMO-LUMO energy gaps

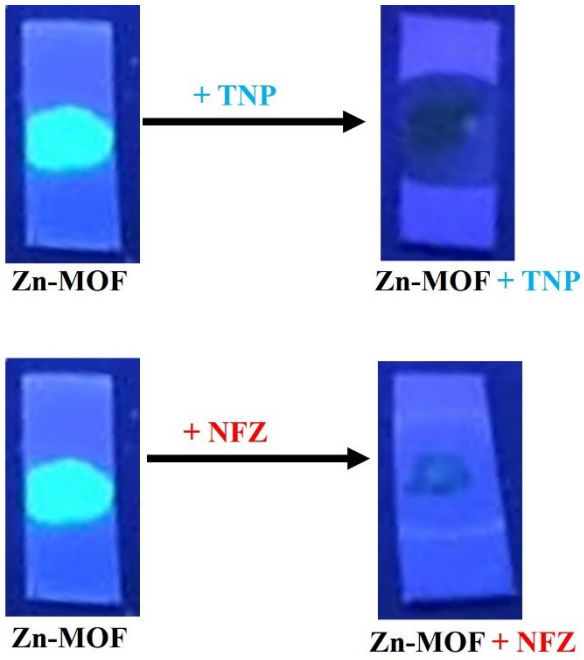

Fig. S35. Fluorescent photograph of the Zn-MOF test strips under UV light (365 nm) illumination in the presence of TNP and NFZ

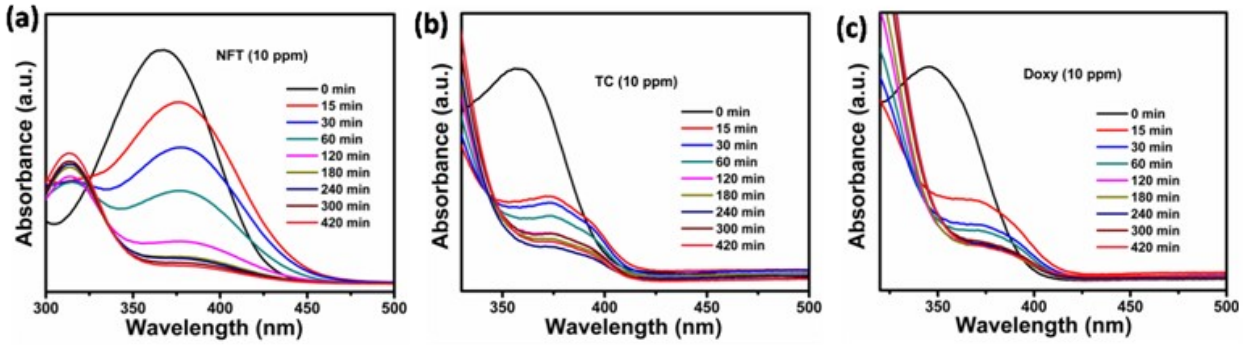

Fig. S36. UV-vis spectra for the adsorption of antibiotics using Zn-MOF (a) NFT, (b) TC and (c) Doxy

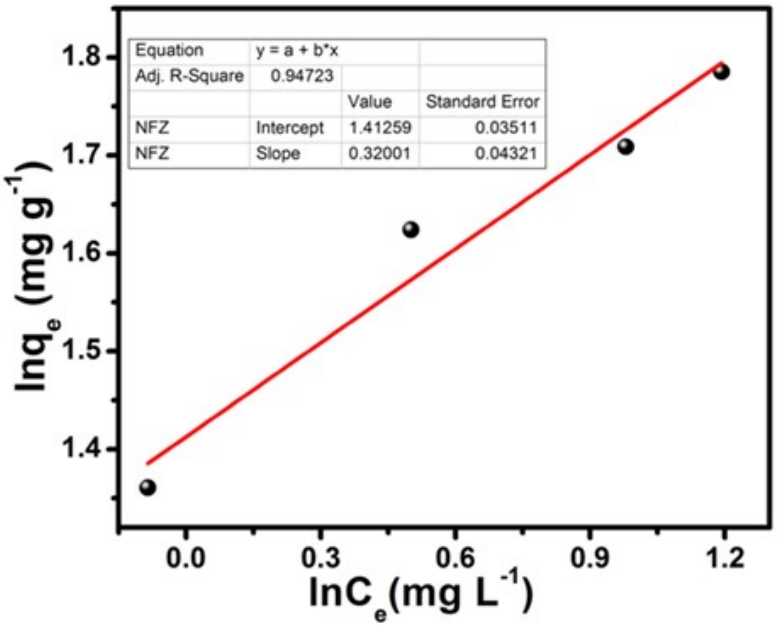

Fig. S37. Plot for fitting of NFZ adsorption experimental data with Freundlich model

Table S8. Parameters of adsorption isotherms of NFZ on Zn-MOF

	Isotherm	**Adj. R^2**	**Other parameters**
NFZ	Langmuir	0.9856	q_m = 66.269 mg g^{-1} b = 0.5306 L mg^{-1}
	Freundlich	0.9472	n = 3.125 k_f = 4.106 (mg g^{-1}(L $mg^{-1})^{1/n}$)

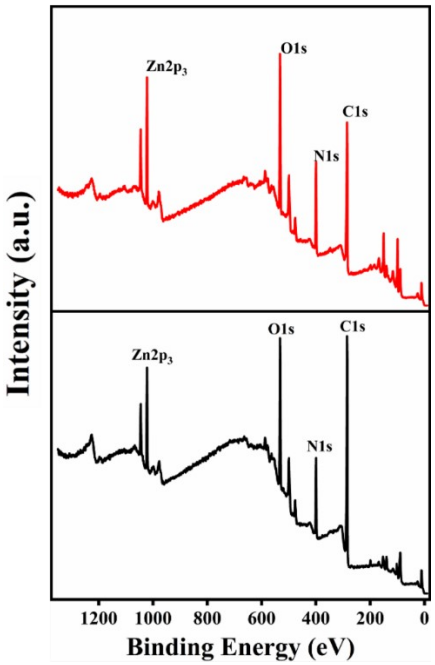

Fig. S38. XPS Survey spectra of Zn-MOF before and after adsorption

Table S9. Comparison q_{max} of NFZ with other reported materials

S.No.	Materials	Analyte	q_{max} (mg/g)	Adsorption (%)	Ref.
1.	Zr-fcu-sti	NFZ	98	N.A	37
2.	$\{[Cd(L)_{0.5}(bpe)_{0.5}(H_2O)]\cdot x(solv)\}_n$	NFZ	16.78	N.A	38
	MOF-1@MF composite	NFZ	47.75		
3.	Multi-walled carbon nanotubes	NFZ	38.215	96.8	39
	Powder-Activated Carbon	NFZ	40.8148	94.7	
4.	Bentonite/magnetite composite	NFZ	27.54 (0.139 mmol/g)	65	40
5.	Tb-MOF	NFZ	N.A	84.4	41
6.	**Zn-MOF**	**NFZ**	**66.269**	**87.42**	**This work**

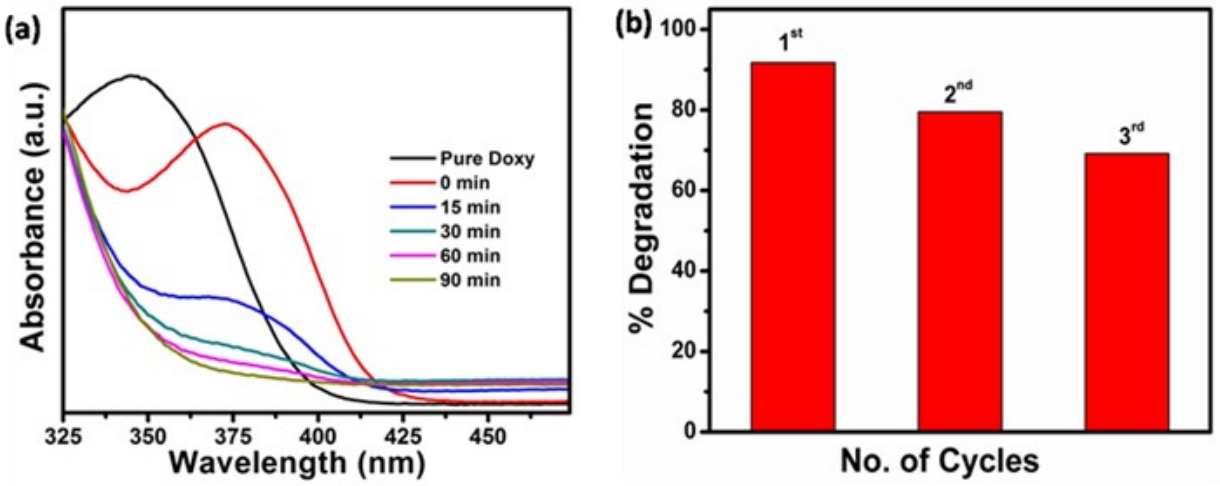

Fig. S39. (a) UV-vis spectra for the photocatalytic degradation of Doxy using Zn-MOF and (b) Reusability plot for degradation of TC using Zn-MOF

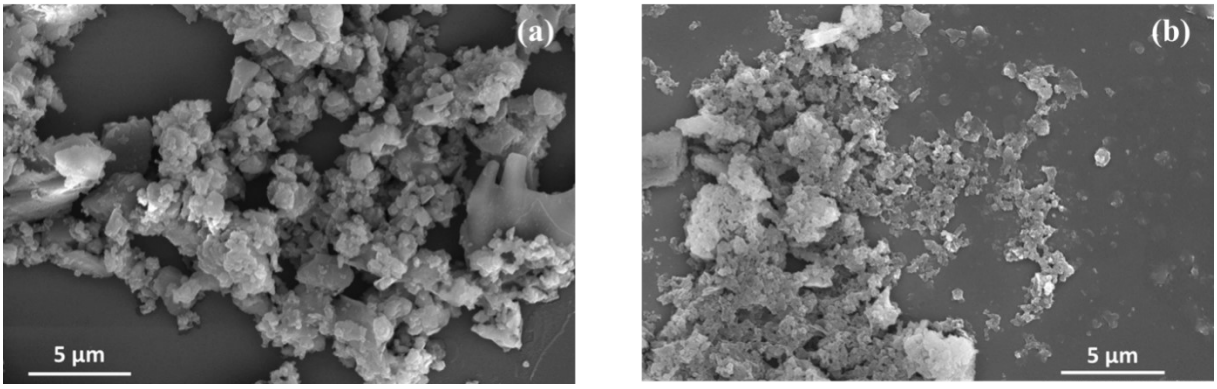

Fig. S40. SEM images of Zn-MOF (a) after adsorption and (b) degradation experiments

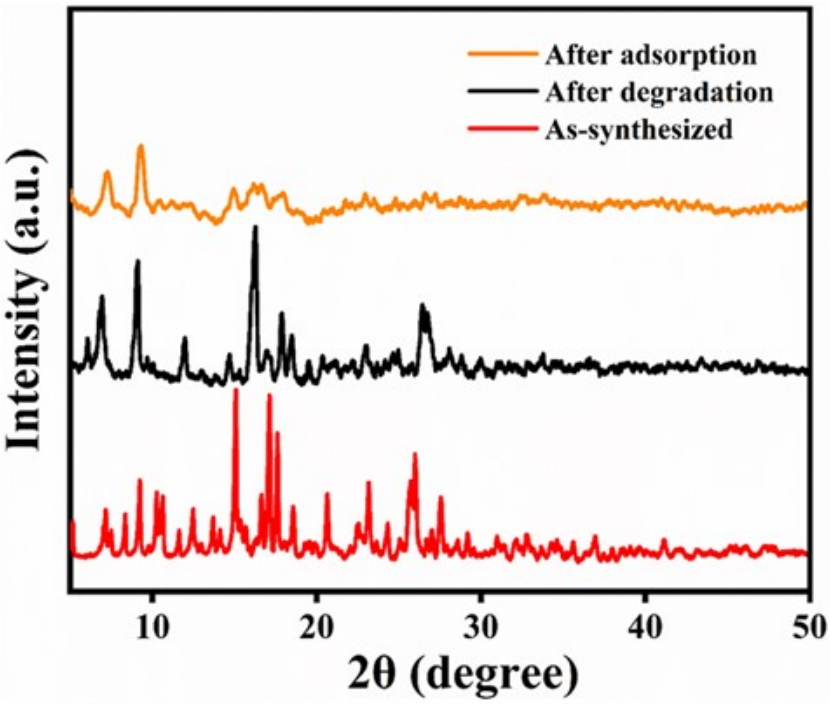

Fig. S41. PXRD patterns of Zn-MOF as-synthesized and recovered after degradation and adsorption experiments

References

1. N. Xu, Q. Zhang and G. Zhang, *Dalton Trans.*, 2019, **48**, 2683-2691.
2. H. Kaur, S. Walia, A. Karmakar, V. Krishnan and R. R. Koner, *J. Environ. Chem. Eng.*, 2022, **10**, 106667.
3. S. Grimme, S. Ehrlich and L. Goerigk, *J. Comput. Chem.*, 2011, **32**, 1456-1465.
4. D. Andrae, U. Haeussermann, M. Dolg, H. Stoll and H. Preuss, *Theor. Chim. Acta.*, 1990, **77**, 123-141.
5. M. e. Frisch, G. Trucks, H. Schlegel, G. Scuseria, M. Robb, J. Cheeseman, G. Scalmani, V. Barone, G. Petersson and H. Nakatsuji, *Inc. Wallingford, CT*, 2016.
6. N. Li, L. Zhou, X. Jin, G. Owens and Z. Chen, *J. Hazard. Mater.*, 2019, **366**, 563-572.
7. M. R. Azhar, H. R. Abid, H. Sun, V. Periasamy, M. O. Tadé and S. Wang, *J. Colloid Interface Sci.*, 2016, **478**, 344-352.
8. v. c. CrysAlisPro Program, Agilent Technologies, Oxford, 2012., 1–49.
9. G. i. Sheldrick, *Sadabs*, 1996.
10. G. M. Sheldrick, *Acta Crystallogr. C Struct. Chem.*, 2015, **71**, 3-8.
11. L. J. Farrugia, *J. Appl. Crystallogr.*, 2012, **45**, 849-854.
12. A. Spek, *Acta Crystallogr. D.*, 2009, **65**, 148-155.
13. D. Wang, Z. Hu, S. Xu, D. Li, Q. Zhang, W. Ma, H. Zhou, J. Wu and Y. Tian, *Dalton Trans.*, 2019, **48**, 1900-1905.
14. X. Zhang, X. Zhuang, N. Zhang, C. Ge, X. Luo, J. Li, J. Wu, Q. Yang and R. Liu, *CrystEngComm.*, 2019, **21**, 1948-1955.
15. A.-M. Zhou, H. Wei, W. Gao, J.-P. Liu and X.-M. Zhang, *CrystEngComm*, 2019, **21**, 5185-5194.
16. S. A. A. M. Razavi, Ali and M. Piroozzadeh, *Inorg. Chem.*, 2022, **61**, 7820–7834.
17. Y. Liu, Y. Wang, Y. Zhang, P. G. Karmaker, L. Zhang, F. Huo, X. Yang and B. Zhao, *Dyes Pigm.*, 2022, **199**, 110099.
18. X. Zhang, Y. Yan, F. Chen, G. Bai, H. Xu and S. Xu, *Z. Anorg. Allg. Chem*, 2021, **647**, 759-763.
19. D. Chakraborty, S. Bej, S. Sahoo, S. Chongdar, A. Ghosh, P. Banerjee and A. Bhaumik, *ACS Sustain. Chem. Eng.*, 2021, **9**, 14224-14237.
20. S. Singh Dhankhar, N. Sharma, S. Kumar, T. Dhilip Kumar and C. Nagaraja, *Chem. Eur. J.*, 2017, **23**, 16204-16212.
21. Z.-W. Zhai, S.-H. Yang, M. Cao, L.-K. Li, C.-X. Du and S.-Q. Zang, *Cryst. Growth Des.*, 2018, **18**, 7173-7182.
22. I. E. Khalil, T. Pan, Y. Shen and W. Zhang, *Inorg. Chem. Commun.*, 2020, **120**, 108170.
23. M.-M. Chen, X. Zhou, H.-X. Li, X.-X. Yang and J.-P. Lang, *Cryst. Growth Des.*, 2015, **15**, 2753-2760.
24. Z. Sun, Y. Li, Y. Ma and L. Li, *Dyes Pigm.*, 2017, **146**, 263-271.
25. X.-S. Wang, L. Li, D.-Q. Yuan, Y.-B. Huang and R. Cao, *J. Hazard. Mater.*, 2018, **344**, 283-290.
26. Q. Hu, T. Xu, J. Gu, L. Zhang and Y. Liu, *CrystEngComm*, 2022, **24**, 2759-2766.
27. S. Yang, J. Hu, J. Zhang, T. He, L. Zhang and H. Chen, *Inorganica Chim. Acta.*, 2022, **536**, 120914.
28. X.-Y. Guo, F. Zhao, J.-J. Liu, Z.-L. Liu and Y.-Q. Wang, *J. Mater. Chem. A.*, 2017, **5**, 20035-20043.
29. L.-L. Ren, Y.-Y. Cui, A.-L. Cheng and E.-Q. Gao, *J. Solid State Chem.*, 2019, **270**, 463-469.
30. D. Zhao, X.-H. Liu, Y. Zhao, P. Wang, Y. Liu, M. Azam, S. I. Al-Resayes, Y. Lu and W.-Y. Sun, *J. Mater. Chem. A* . 2017, **5**, 15797-15807.
31. Z. Lei, L. Hu, Z.-H. Yu, Q.-Y. Yao, X. Chen, H. Li, R.-M. Liu, C.-P. Li and X.-D. Zhu, *Inorg. Chem. Front.*, 2021, **8**, 1290-1296.
32. S.-L. Hou, J. Dong, X.-L. Jiang, Z.-H. Jiao, C.-M. Wang and B. Zhao, *Anal. Chem.*, 2018, **90**, 1516-1519.

33. S. Xu, J.-J. Shi, B. Ding, Z.-Y. Liu, X.-G. Wang, X.-J. Zhao and E.-C. Yang, *Dalton Trans.*, 2019, **48**, 1823-1834.
34. Y. Yang, G. Ren, W. Yang, X. Qin, D. Gu, Z. Liang, D.-Y. Guo and P. Qinhe, *Polyhedron*, 2021, **194**, 114923.
35. Y.-L. Xu, Y. Liu, X.-H. Liu, Y. Zhao, P. Wang, Z.-L. Wang and W.-Y. Sun, *Polyhedron*, 2018, **154**, 350-356.
36. B. Li, Q. Lei, F. Wang, D. Zhao, Y. Deng, L. Yang, L. Fan and Z. Zhang, *J. Solid State Chem.*, 2021, **298**, 122117.
37. P. Su, A. Zhang, L. Yu, H. Ge, N. Wang, S. Huang, Y. Ai, X. Wang and S. Wang, *Sens. Actuators B: Chem.*, 2022, **350**, 130865.
38. M. Lei, F. Ge, S. Ren, X. Gao and H. Zheng, *Sep. Purif. Technol.* , 2022, **286**, 120433.
39. W. Ying-Ying and X. Zhen-Hu, *J Dispers Sci Technol* . 2016, **37**, 613-624.
40. O. V. Alekseeva, A. N. Rodionova, A. V. Noskov and A. V. Agafonov, *Clays Clay Miner.*, 2019, **67**, 471-480.
41. J. Zhang, L. Gao, Y. Wang, L. Zhai, X. Niu and T. Hu, *CrystEngComm.*, 2019, **21**, 7286-7292.